UPPSALA
UNIVERSITET

Digital Comprehensive Summaries of Uppsala Dissertations from the Faculty of Medicine 1846

Image-based multi-omics data integration

Exploring whole-body PET/MRI, -omics data and body composition

ROBIN VISVANATHAR

ACTA
UNIVERSITATIS
UPSALIENSIS
UPPSALA
2022

ISSN 1651-6206
ISBN 978-91-513-1517-1
URN urn:nbn:se:uu:diva-473349

Dissertation presented at Uppsala University to be publicly examined in Föreläsningssalen, Röntgen, Akademiska Sjukhuset, ingång 70, Uppsala, Monday, 13 June 2022 at 08:00 for the degree of Doctor of Philosophy (Faculty of Medicine). The examination will be conducted in English. Faculty examiner: Professor Katrine Riklund (Umeå universitet).

Abstract
Visvanathar, R. 2022. Image-based multi-omics data integration. Exploring whole-body PET/MRI, -omics data and body composition. *Digital Comprehensive Summaries of Uppsala Dissertations from the Faculty of Medicine* 1846. 61 pp. Uppsala: Acta Universitatis Upsaliensis. ISBN 978-91-513-1517-1.

Advanced body composition analysis with whole-body imaging could uncover novel associations between regional tissue composition and metabolic disease. Imiomics is an automated image analysis framework that enables large-scale integration of magnetic resonance imaging (MRI) data and orthogonal technologies such as metabolomics and genomics for the detailed study of body composition. The Imiomics method is based on spatial normalisation to attain voxel-to-voxel correspondence in large cohorts of volumetric MR images. The spatially normalised data is then further used to generate voxel-wise statistical inference volumes for analysis. In this thesis, Imiomics was integrated with metabolomics for the first time, providing a detailed map of the relationship between the metabolome and regional body composition in T2D. Furthermore, Imiomics was integrated with genomics for the first time, exposing detailed associations between single nucleotide polymorphisms (SNPs) and sex-stratified body composition. A rapid and intuitive visual framework was developed for the analysis of volumetric Imiomics maps, and further applied to study the relationship between body composition and clinical variables in T2D. Whole-body positron emission tomography (PET)/MR was used to study detailed insulin-stimulated glucose metabolism and its associations with tissue volume and tissue fat fraction. This thesis has contributed to the field of advanced body composition research, primarily through the integration of Imiomics with additional -omics platforms.

Keywords: Body composition, Imiomics, genomics, metabolomics, MRI, PET, insulin sensitivity, T2D

Robin Visvanathar, Department of Surgical Sciences, Akademiska sjukhuset, Uppsala University, SE-75185 Uppsala, Sweden.

ISSN 1651-6206
ISBN 978-91-513-1517-1
URN urn:nbn:se:uu:diva-473349 (http://urn.kb.se/resolve?urn=urn:nbn:se:uu:diva-473349)

To my family

List of Papers

This thesis is based on the following papers, which are referred to in the text by their Roman numerals.

I. Diamanti K*, **Visvanathar R*,** Pereira M, Cavalli M, Pan G, Kumar C, Skrtic S, Risérus U, Eriksson JW, Kullberg J, Komorowski J, Wadelius C, Ahlström H. (2020) Integration of whole-body [18F]FDG PET/MRI with non-targeted metabolomics can provide new insights on tissue-specific insulin resistance in type 2 diabetes. *Scientific Reports*.

II. Eriksson JW, **Visvanathar R**, Kullberg J, Strand R, Skrtic S, Ekström S, Lubberink M, Lundqvist MH, Katsogiannos P, Pereira MJ, Ahlström H. (2021) Tissue-specific glucose partitioning and fat content in prediabetes and type 2 diabetes: whole-body PET/MRI during hyperinsulinemia. *European Journal of Endocrinology*.

III. **Visvanathar R**, Carlbom L, Ekström S, Strand R, Skrtic S, Pereira MJ, Eriksson JW, Ahlström H, Kullberg J. Exploration of whole-body PET/MRI and clinical variables in type 2 diabetes for data-driven hypothesis generation. *Manuscript*.

IV. **Visvanathar R**, Censin J, Menzel U, Ahman S, Malmberg F, Kullberg J, Fall T, Ahlström H. Genetic variation and sex-stratified advanced body composition analysis: neck-to-knee MRI and genetics in the UK Biobank. *Manuscript*.

* These authors contributed equally to this work as first authors.

Figure 5. PET/MRI can provide detailed tissue-specific information on glucose uptake. From left to right: PET image (glucose uptake), MRI (adipose tissue signal) and MRI (water signal)

4. The ‘Omics’ Era

The hour-long ‘central dogma’ lecture was held by Nobel Prize laureate Francis Crick in September 1957[36]. During the lecture Crick shared his understanding of the flow of genetic information from gene to protein. The lecture gave birth to what nowadays is recognised as “the central dogma of molecular biology”, though, the original notes[37] shared by Crick have been largely misquoted.

> This states that once ‘information’ has passed into protein it cannot get out again. In more detail, the transfer of information from nucleic acid to nucleic acid, or from nucleic acid to protein may be possible, but transfer from protein to protein, or from protein to nucleic acid is impossible.
>
> **Crick, F.H.C., *On protein synthesis*, p. 152, 1958.**

Congruent with past misquotation through abstraction, **Figure 6** illustrates a modified representation of the central dogma. **Paper I** and **IV** aimed not only to understand how information flows from genes to proteins, but rather from metabolites to disease phenotype and genes to body composition, respectively.

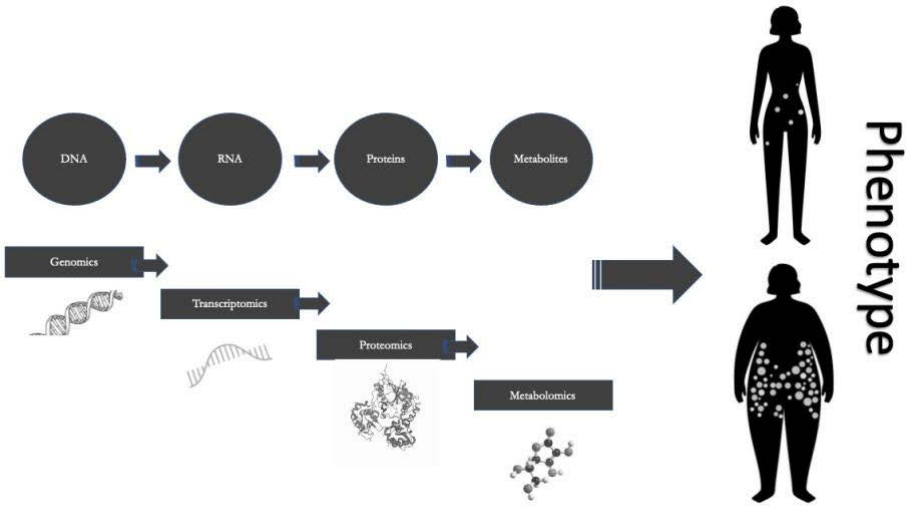

Figure 6. The central dogma in the age of -omics and body composition.

The number of -omics publications have significantly increased in the last few years as high-throughput technologies have been made more accessible to researchers (**Figure 7**). In addition, the tools required for big data processing have considerably improved, largely due to open-source initiatives[38,39].

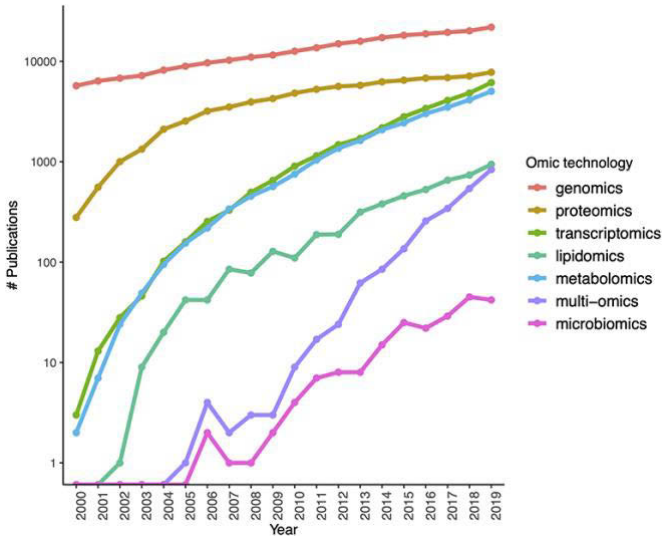

Figure 7. The number of publications on PubMed mentioning -omics technologies from 2000 to 2019. Figure adapted with CC BY 4.0. Anda-Jáuregui & Hernández-Lemus, (2020).

4.1 Genome-wide association studies and phenotypes

The objective of functional genomics is to explore how the genome together with a multitude of complex interactions contribute to specific phenotypes[38]. A common experimental design to study the associations between genetic variants and phenotypes is genome-wide association studies (GWAS). Single-nucleotide polymorphisms (SNPs) are genotyped using DNA (micro)arrays where hybridisation of immobilised oligonucleotides and labelled sample DNA produce fluorescent signals that can be detected and quantified. The technology has rapidly improved, specifically through the parallelisation of solid support-based oligonucleotide hybridisation[39,40]. Millions of SNPs can be measured with a reasonable degree of effort and cost, and untyped SNPs can be tagged by using a range of statistical methods (e.g., linkage disequilibrium and imputation) to attain genome-wide coverage[41].

According to Hirschhorn & Gajdos[42], the first broadly replicable GWAS was published in *Science* by Klein et al. in 2005, detailing the connection between a polymorphism in the complement factor H gene and age-related macular degeneration[43]. Since then the field has boomed, and hundreds of complex phenotypes have been linked to thousands of SNPs[44]. Disease-

associated SNPs have been reported for T2D[45,46], inflammatory bowel disease[47,48], rheumatoid arthritis[49], low-density lipoprotein (LDL)-cholesterol[50], osteoporosis[51] and many more[44]. Significant contributions of GWAS also include the discovery of the obesity gene, *FTO* (fat mass and obesity associated gene)[52,53]. However, the significance and utility of GWAS results have been challenged by several prominent scientists. Opposing thoughts emphasise the limited effect sizes typically reported in GWAS, lack of causality and the overflowing spurious findings[54–57]. The large amount of experimental data produced with GWAS poses significant challenges for researchers to maintain proper quality control (QC) procedures and statistical rigor.

Challenges associated with GWAS are particularly evident when studying complex traits such as body composition phenotypes[58]. In other words, the genetic variation that meaningfully contributes to complex traits is seldom attributed to an isolated polymorphism at a single locus. The associations between several individual SNPs and body composition were studied in **Paper IV**, in addition, polygenic risk scores (PRS) were included to address some of the concerns with GWAS and complex traits. PRS address the limitations of individual SNPs by combining a set of independent variants, commonly as a weighted sum according to

$$\boldsymbol{PRS} = \sum_{i}^{N} \boldsymbol{\beta}_{i} \times \boldsymbol{dosage}_{ij}, \tag{4.1}$$

where N represents the number of SNPs included in the PRS, β is the effect size and $dosage_{ij}$ is the copy number of SNP *i* in individual *j*[59]. Several additional approaches for calculating PRS exist, which is further considered in **Paper IV** where two different methods were used[58–60].

4.2 Mass spectrometry-based metabolomics

The road from gene/s to phenotype is long and convoluted, and whilst there are many -omics technologies (e.g., transcriptomics, proteomics and lipidomics) available for the study of downstream events, metabolic pathways are commonly studied using metabolomics. Products and substrates of metabolism are typically measured with the analytical techniques nuclear magnetic resonance (NMR) spectroscopy or mass spectrometry (MS). A review of the many available analytical techniques and variations thereof is outside the focus of this thesis but the reader is encouraged to read the introductory review by Liu & Locasale[61]. In **Paper I,** metabolites were identified with MS coupled with either liquid chromatography (LC-MS) or gas chromatography (GC-MS). There are many differences between the two techniques, an important consideration in **Paper I** was that the coverage is

different, as such when used together LC-MS and GC-MS provide broader metabolite coverage (**Figure 8**)[62].

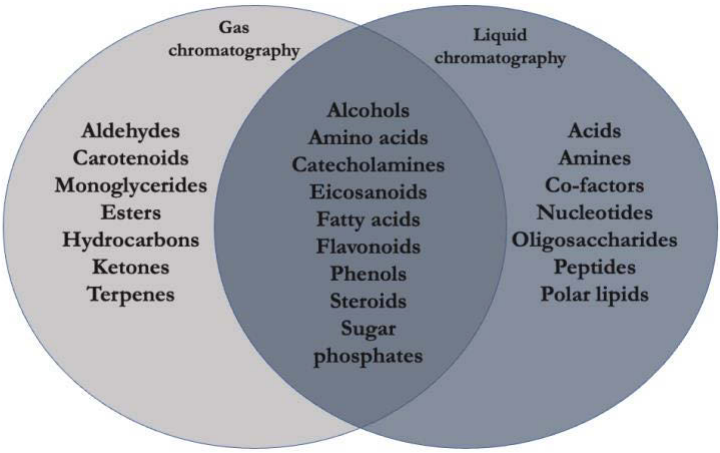

Figure 8. Venn diagram illustrating the different metabolite classes that are covered by GC-MS and LC-MS, respectively.

A simplified MS workflow is illustrated in **Figure 9**. The mass-to-charge ratio (m/z), relative abundance and retention time (RT) are collected for each parent ion, and if tandem mass spectrometry is used (e.g., LC-MS/MS) a downstream fragmentation step provides the respective features for the fragment ions[63,64]. In very simple terms for the non-initiated, metabolites are separated using GC or LC and afterwards MS is used to detect them based on mass. The extracted features are used for metabolite profiling, which depending on the experimental design can be targeted or untargeted. Even for experienced bioinformaticians in the field, processing and matching raw MS data to metabolites is non-trivial. Open-source software packages are commonly used in metabolomics research, these tools apply advanced methods for peak identification, alignment, deconvolution and more[65]. Finally, metabolites can be identified using publicly available databases or in-house libraries[66,67].

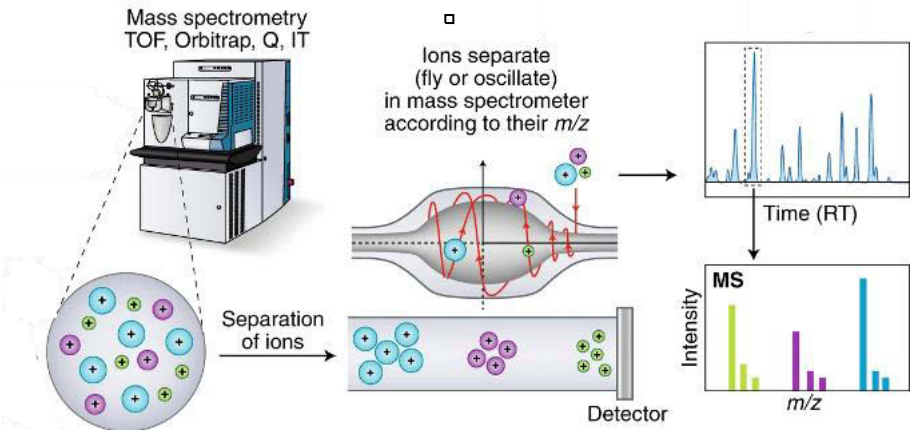

Figure 9. Simplified overview of mass-spectrometry workflow. Adapted with permission from Springer Nature. Alseekh et al. (2021).

Metabolomics is a useful technology for studying variability in body composition and metabolic dysfunction in diseases such as T2D[68]. A series of exploratory metabolomics studies have reported associations between T2D and bile acids[69], aromatic amino acids (AAAs)[70], branched-chain amino acids (BCAAs)[71] and phospholipids[72]. The technology can further be used for predictive modelling of disease progression or development, this was illustrated in a seminal paper by both Wang et al., and Liu et al. in decade-long follow-up studies[71,73]. Though, the relative additional value of these models compared with standard clinical risk factors (e.g., BMI, FPG and HbA1c) warrants additional study.

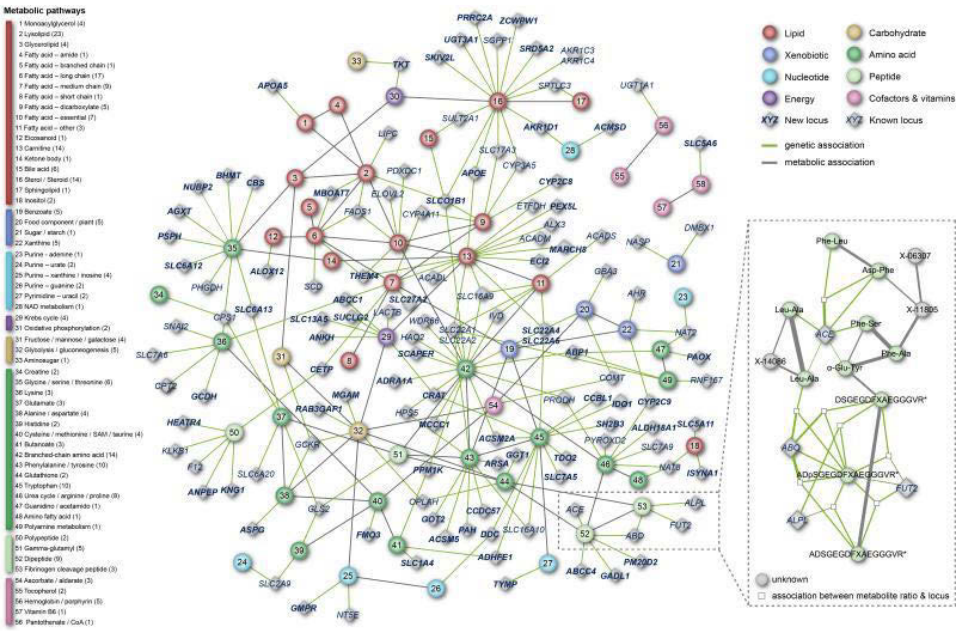

Figure 10. A systems biology approach to study metabo-genomics, sometimes referred to as mGWAS. Reprint with permission from Springer Nature. Shin et al., (2014).

Systems biology approaches aim to integrate untargeted metabolomics with other -omics technologies to reveal novel insights into the biological relevance of the results from exploratory metabolomics studies[75–77]. To demonstrate this in a comprehensive exploratory study, Shin and colleagues combined GWAS and metabolomics to map the genetic influences of the human metabolome and reported 84 novel metabolic loci (**Figure 10**)[74]. Metabolite genetics, sometimes referred to as mGWAS[78], has now been used in numerous studies to characterise the genetic influence on metabolic phenotypes[79–81]. Conversely, few studies have reported the associations between metabolites and whole-body tissue composition. In **paper I**, metabolomics was integrated with the Imiomics framework for the first time with the objective to explore novel hypothesis-generating insights.

5. Medical Imaging

The previous chapters discussed the implications of detailed body composition studies in partnership with -omics technologies. In this chapter, the medical imaging techniques that were used in **Paper I-IV** are discussed in more detail.

5.1 Basics of magnetic resonance imaging (MRI)

In **chapter 4**, NMR was mentioned for its use in metabolomics research. The technology was first documented by Nobel Prize laureate Isidor Isaac Rabi in 1939, although towards the end of World War II independent contributions by Nobel Prize laureates Felix Bloch and Edward M. Purcell extended the capabilities of the technology[82,83]. A third Nobel Prize was awarded many years later to Paul Lauterbur and Peter Mansfield for the development of MRI, where NMR signals were used to create 2-D images[84].

Amongst the many relevant elements in the body (e.g., ^{1}H, ^{16}O, ^{23}Na, $^{14}N$and ^{31}P), hydrogen nuclei have the strongest NMR signal. Hydrogen is also the most relevant for clinical MRI due to the high abundance in adipose tissue and water. The intrinsic nuclear angular momentum (spin) property of hydrogen nuclei determines its behaviour in the presence of a strong external magnetic field. In a MR system, a strong static magnetic field, $\mathbf{B_0}$, is used to align hydrogen nuclei with the direction of $\mathbf{B_0}$ and induce a net magnetisation, **M**, in the tissue. Subsequently, a weaker magnetic field, $\mathbf{B_1}$, is used to temporarily perturb the direction of **M** away from the longitudinal plane to the transverse plane[83]. This is achieved by the transmission of a radiofrequency (RF) pulse at the resonance frequency of **M,** resulting in the absorption of energy by the hydrogen nuclei and the ability to flip their alignment away from the direction of $\mathbf{B_0}$. As **M** approaches equilibrium i.e., as the hydrogen nuclei following RF excitation returns to a resting state (relaxation), RF waves are emitted from the tissues and measured using receiver coils. The signals then undergo a series of image reconstruction steps, including a Fourier transformation, to transform the raw data into MR images as depicted in **Figure 11**[83,85–88].

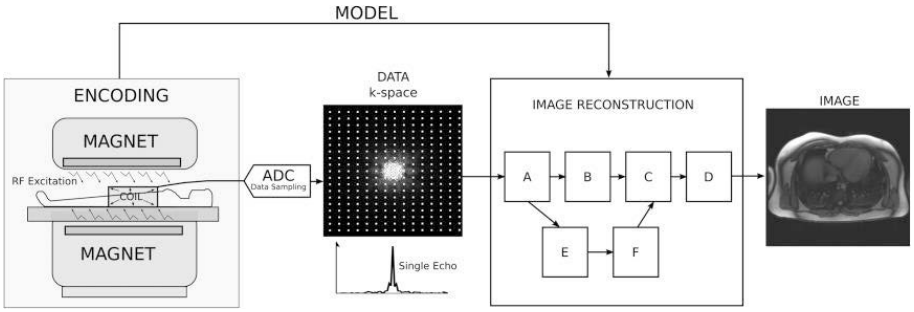

Figure 11. Overview of the image acquisition and reconstruction process in MRI. Adapted with permission from John Wiley and Sons. Hansen & Kellman (2015).

5.1.1 The Dixon method

Many parameters can be adjusted to generate different types of MR images. Importantly, relaxation times are different between tissues, a property which is commonly exploited to provide tissue contrast in MRI. MRI provides exceptional soft tissue contrast compared with other imaging techniques. However, body composition studies can benefit from auxiliary separation of the adipose tissue- and water signal. Generally, this can be achieved by suppressing the signal from adipose tissue by using the versatile Dixon technique[89]. The Dixon technique takes advantage of the fact that hydrogen nuclei have different resonance frequencies in water and adipose tissue, sometimes referred to as the chemical shift difference. The chemical shift difference translates into a phase difference as a function of the echo time, hence by acquiring images when the water- and adipose tissue signals are in-phase (IP) and out-of-phase (OOP), one can reconstruct water-only images and adipose tissue-only images as illustrated in **Figure 12**[90].

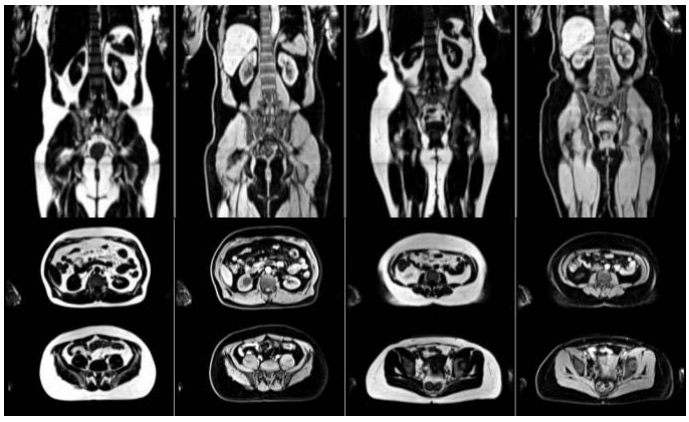

Figure 12. Adipose tissue and water separated MRI using the Dixon method. From left to right: adipose tissue signal (male), water signal (male), adipose tissue signal (female), water signal (female)

5.2 Basics of positron emission tomography (PET)

The basic principles of PET are based on the detection of electron-positron annihilation events[91]. Briefly, annihilation events are initiated by radionuclide decay resulting in the emission of a positron (β^+) and a neutrino (v). The decay occurs as the unstable radioactive isotope transitions from a high-energy state to a lower-energy state. When the positron eventually collides with an electron in the tissue, an annihilation event occurs, where both masses are turned into energy according to Einstein's equation

$$\boldsymbol{E = mc^2}. \tag{5.1}$$

Two high-energy (511 keV) photons are created and emit in opposite directions. The high-energy photons are picked up by pairs of colinearly aligned detectors, converted to an electrical signal, amplified and the raw data finally processed with image reconstruction algorithms (**Figure 13**)[91].

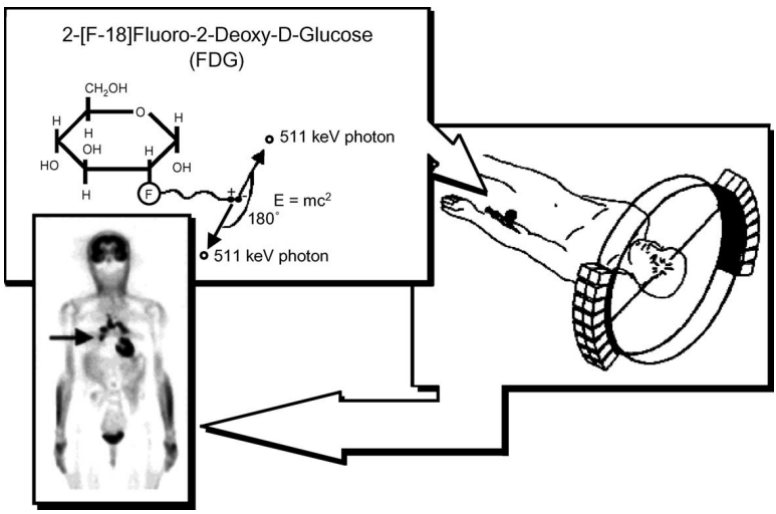

Figure 13. Simplified overview of the PET image acquisition process. Reprint with permission for Elsevier. Walker et al. (2004)

5.3 Integrated PET/MRI

PET is a quantitative functional imaging technique, but it offers limited anatomical information. It is an ideal orthogonal technique for successful integration with MRI, which was the method used for data acquisition in **paper I-III**. In oncology, ^{18}F-fluorodeoxyglucose (FDG) PET/computer tomography (CT) is frequently used. PET/MRI offers several advantages compared with PET/CT, including superior soft tissue contrast, lower ionizing

radiation and the option of multiparametric or functional imaging (e.g., diffusion-weighted imaging)[92]. Weaknesses of PET/MRI compared with PET/CT include but are not limited to, longer acquisition times, higher cost of integrated PET/MR systems and challenges with attenuation correction (AC)[93]. AC is a key challenge for PET/MRI. Simply put, when our previously mentioned opposing 511 keV proton-pair travel through the tissue they might interact with electrons and change direction (loss of energy), resulting in the attenuation of the PET signal[94]. Photon attenuation can be described according to

$$\frac{I}{I_0} = e^{-\mu L}, \tag{5.2}$$

where the non-attenuated signal (I) could be recovered should the other variables (I_0 - attenuated signal, μ - linear attenuation coefficient and L – tissue thickness) be known[94]. Unfortunately, MRI struggles with generating the required linear attenuation coefficient maps (μ maps), conversely, transforming CT Hounsfield Units (HU) to μ values is simpler because CT is fundamentally based on the attenuation of x-rays. MR-based attenuation correction (MRAC) is a well-researched field with continuous innovations hoping to solve the challenges associated with PET/MRI[95,96]. The Dixon technique is commonly applied, followed by image segmentation to acquire predefined μ values for specific tissues[97].

In summary, several publications have reported extended comparisons between PET/CT and PET/MRI, predominantly in the context of oncology[92,93]. For metabolic body composition studies ^{18}F-FDG PET/MRI is superior because of the exceptional soft tissue contrast and low radiation exposure, despite its current challenges.

6. Medical Image Analysis

Basic principles help us understand the image acquisition process in MRI and PET, but ultimately the acquired raw data is transformed into a digital image in a process termed *image reconstruction*. A review of the intricacies of image reconstruction is outside the scope of this thesis, however, two noteworthy general concepts are worth mentioning: sampling and quantisation. With sampling and quantisation an analogue image is transformed into a digital image. The two processes determine the spatial- and gray level resolution of the digitised image. In this thesis, the work has been focused on monochrome (grayscale) and binary images (black and white). Typical image sizes were 362x155x224, containing 12,568,640 'voxels' for statistical inference.

6.2 Imiomics – an overview

The aim with Imiomics is to attain voxel-to-voxel correspondence of whole-body MR images to enable unbiased voxel-wise statistical inference and additional subsequent applications[98].

6.2.1 Image registration

The spatial normalisation i.e., the deformation of images to a common coordinate system is accomplished by using a three-step image registration process. The framework utilises the complementary information in acquired water- and adipose tissue separated MR images. Assumptions of tissue variability between subjects motivates the step-by-step registration process. The between-subject variability of bone is assumed to relatively low due to its rigid structure, in contrast, adipose tissue inter-variability is assumed to be relatively high and lean tissue inter-variability falls somewhere in the middle. Spatially varying tissue elasticity constraints are used to reflect these assumptions where the bones are registered first followed by lean tissue and lastly adipose tissue, each subsequent step constrained by the previous one/s (**Figure 14)**[98].

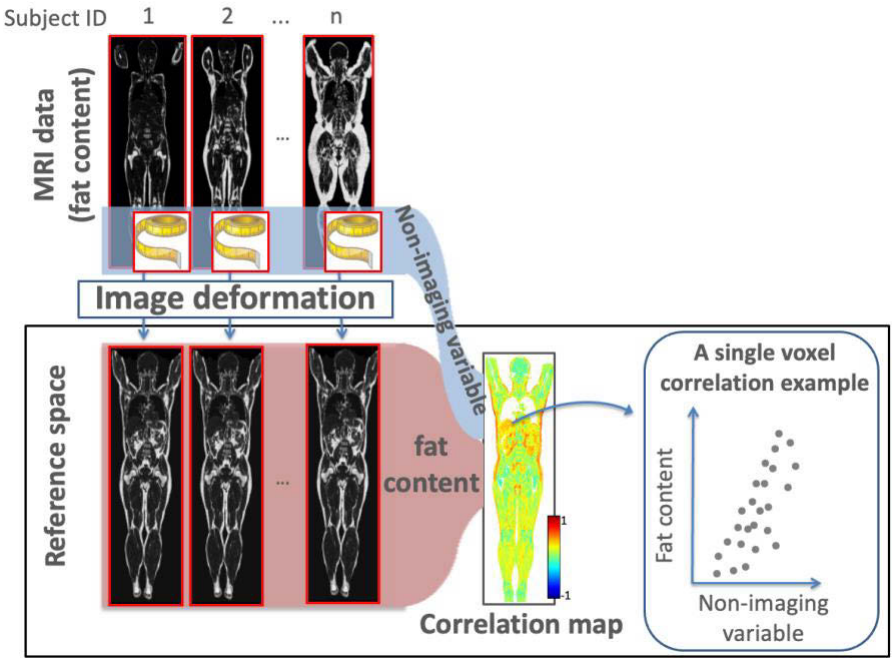

Figure 14. An illustration of the Imiomics workflow from MRI data to correlation maps. Figure adapted with support from Joel Kullberg and Robin Strand.

Accurately evaluating the registration results is challenging, three different methods have been used:

i. Visual evaluation of the registered images

ii. Inverse consistency as given by

$$\boldsymbol{T}_{A_i \to B} \circ \boldsymbol{T}_{B \to A_i} \; \boldsymbol{and} \; \boldsymbol{T}_{B \to A_i} \circ \boldsymbol{T}_{A_i \to B}, \tag{6.1}$$

in basic terms, the registration method should ideally be insensitive to the source/target arrangement of the image pair.

iii. The Dice similarity coefficient as given by

$$\boldsymbol{DSC} = \frac{\boldsymbol{2} \times |\boldsymbol{A} \cap \boldsymbol{B}|}{|\boldsymbol{A}| + |\boldsymbol{B}|}, \tag{6.2}$$

in the binary setting[99]. It was used to evaluate image segmentations of water- and adipose tissue[98].

Since simultaneous acquisition of PET/MR images produces inherently co-registered images, the deformation fields from the MR registration can be used on the corresponding PET image when applying Imiomics to PET/MRI.

6.2.2 Image segmentation

Medical image segmentation refers to the process of delineating regions of interest (ROI) in medical images[100]. In the simplest case, the annotation process results in a binarized image, *segmentation mask*, where pixels of interest are labelled as 1s and background pixels are 0s. The spatial normalisation feature of Imiomics enables atlas-based image segmentation, where segmentation masks from the reference volume (single-atlas) or volumes (multi-atlas) are propagated to unlabelled images. In addition to Imiomics, many other methods are available for automating the image segmentation process. In recent years, deep learning has predominantly taken over. The most impactful paper in the medical image segmentation field during the last decade has arguably been "*U-Net: Convolutional Networks for Biomedical Image Segmentation*" by the Google DeepMind research scientist Olaf Ronneberger et al.[101]. The U-Net, an encoder-decoder model, is incredibly powerful and easy to use, with countless variations depending on the specific task[102]. Imiomics is different from deep learning in that it enables holistic analysis of the whole-body image. In addition, as deformation fields are stored, there is a greater degree of traceability with Imiomics compared to powerful but relatively black-boxed deep learning models. Developments within the medical image deep learning field, particularly the focus on explainable AI and transfer learning will result in the increased use of deep learning for all sorts of medical applications. Deep learning could also be incorporated into Imiomics to further advance image registration efforts[103,104].

6.2.3 Voxel-wise statistical inference

The Swedish National Infrastructure for Computing (SNIC) provides high-performance computing (HPC) resources to researchers working with sensitive data. In Uppsala, Sweden, the research system Bianca is maintained and further developed by Uppsala Multidisciplinary Centre for Advanced Computational Science (UPPMAX). Bianca and its 204 compute nodes with a total of 3264 cores, was made available to our research group for parts of this thesis, the computational resources enabled increasingly large-scale studies to be performed using Imiomics.

Voxel-wise statistical inference following image registration is a computationally costly process. The procedure involves iteratively loading large image files from disk into memory, saving parts of the image volume (V_p) depending on the total number of files, file size and available memory, and then loading the next file until all image volumes have been included. The process then repeats n-times, where n is the total image volume/V_p, until the full volume has been processed for each image file. Finally, combined output volumes are generated (e.g., Pearson correlation coefficient, *r*, maps). Significant optimisation and method development work was completed for this thesis. Two internal codebases are currently maintained for optimizing

voxel-wise statistical inference calculations using Bianca. For this thesis, primarily **paper III-IV,** a codebase based on memory-mapped files using the numerical python (NumPy*)* package was developed. Briefly, instead of iteratively loading large files n-times and saving small parts of the volumes, a structure for combining all images (3D arrays) into one massive file on disk was considered. Flattening the 3D arrays and horizontally stacking them achieves this (**Figure 15**).

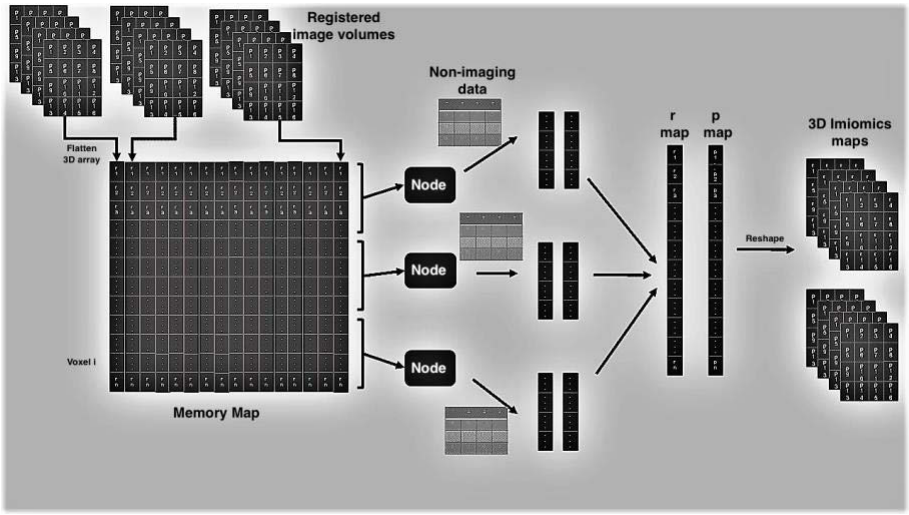

Figure 15. Schematic overview of the voxel-wise statistical inference workflow using a distributed approach.

Next, as memory-mapped files in NumPy allows for partial file reading, this was utilised to 'synchronously' distribute different parts of the file to multiple nodes on Bianca (n=40 used here). The individual outputs from the distributed computing scheme were finally stitched together into the desired Imiomics output volumes (e.g., *r* maps).

Addressing the bottlenecks of iterative image loading by using distributed HPC provides several advantages, some of which were realised for the first time in **Paper IV**. Computationally intensive statistical methods could now be used effectively at scale i.e., instead of computing Pearson correlation coefficients, multiple linear regression models or multi-step multiple linear regression models could be constructed with output volumes representing the R^2, β-coefficients and corresponding p-values. Furthermore, as the loading of independent variables or covariates into memory was completely decoupled from the image loading and distribution, multiple relationships could be studied while the image data is in memory. As demonstrated in **paper IV**, permutation-based multiple comparison correction was performed at scale, removing the dependency on conservative methods such as Bonferroni adjustments in accordance with the results of Breznik et al.[105].

7. Whole-body Imaging, -Omics and Body Composition

7.1 Summary of Imiomics- and associated studies

Imiomics was first introduced by Kullberg et al. at the 23rd Annual Meeting of the International Society for Magnetic Resonance in Medicine (ISMRM) in 2015[106]. A more extensive summary was introduced two years later by Strand et al.[98]. The framework was intended to address the weaknesses of traditional a priori-based whole-body analysis methods where large parts of the image outputs were disregarded. The three-step image registration method was evaluated on 128 individuals from the Prospective investigation of Obesity, Energy and Metabolism (POEM) cohort[107] and a number of example applications were demonstrated for the first time[98]. A second method development paper followed in 2018 by Johansson et al. and confirmed the feasibility of integrated PET/MRI and HEC in 10 participants[34]. The study was completed on a subset of *cohort I* (see **Chapter 8**). An additional report on *cohort I* was presented by Boersma et al., where glucose uptake in T2D was explored, in a similar approach to **Paper II**[108]. Though, there were significant methodological differences between the studies. Boersma et al., was completed on a subset of *cohort I* and only manual segmentations were used, with limited MRI measurements. Conversely, **Paper II** was based on an automatic image analysis method and included complex glucose metabolism features including but not limited to, rate of glucose disappearance (R_d), endogenous glucose production (EGP), total tissue glucose uptake rates (Total MR_{glu}) and glucose partitioning calculations (see **Chapter 9**). Hence, **paper II** was able to address fundamentally different and more detailed questions of adipose tissue and glucose metabolism in T2D. A series of Imiomics studies followed, including works from this thesis, studying body composition and vasoreactivity[109], proinflammatory interleukins[110], metabolic syndrome[111], glucose metabolism[112], metabolomics[113] and intima-media thickness[114]. In addition, several technical development papers have been published describing optimisation of the image registration method and other validation activities[115–119].

7.2 Summary of body composition and GWAS studies

GWAS have discovered hundreds of near-independent significant SNPs associated with BMI[120,121], WHR_{adjBMI}[122], waist circumference[123], lean body mass (LBM)[124] and height[125]. In a recent study, bio-electrical impedance (BIA) was used by Rask-Andersen et al. to study the genetic variation of relative body fat distribution in the arms, legs and trunk[126]. The study identified 98 near-independent SNPs, of which 29 were novel i.e., not previously associated to an adiposity-related phenotype[126]. Dual energy X-ray absorptiometry (DXA) has also been used to study body composition in combination with GWAS in the UK Biobank[13]. From a starting point of 6,137,607 imputed SNPs, the authors retrieved three SNPs (rs7592270, rs77772562 and rs7552312) that were associated with multiple obesity indicators and one (rs2236705) that was associated with a lean phenotype, specifically female lean leg mass. While DXA and BIA are great techniques, MRI is considered the gold standard for advanced body composition research[7]. Nevertheless, few studies have investigated the heritability of body composition phenotypes as measured by whole-body MRI. Recently, Ji et al. integrated GWAS and MRI data from the UK Biobank to study the heritability of a "favourable adiposity phenotype"[127]. Even though the MRI part was limited to a single transverse slice of the liver, the concept of a favourable adiposity phenotype is intriguing and harmonises with the gluteofemoral SAT proponents from **Chapter 1**. To the best of my knowledge, the only GWAS and advanced body composition study that rivals **Paper IV** in sample size is a very recent study from Liu et al. on the UK Biobank[128]. The team from Madeleine Cule's lab used deep learning, specifically a combination of 2D and 3D U-nets[101], to segment and extract fat and iron in VAT, SAT, lungs, spleen, kidney, pancreas and liver from MRI scans in over 38,000 participants.

8. Experimental Design

The work presented in this thesis is based on the extensive study of two cohorts, comprising of several independently acquired orthogonal datasets. The data was acquired and analysed using different technologies, such as the ones already introduced.

8.1 Cohort I

Cohort 1 is the result of a large collaboration study between AstraZeneca, Uppsala University and SciLifeLab. The study involved over 15 collaborators, with the aim to study T2D development through both a vertical and horizontal (interdisciplinary) approach. A summary of the initial study design is represented in **Figure 16**.

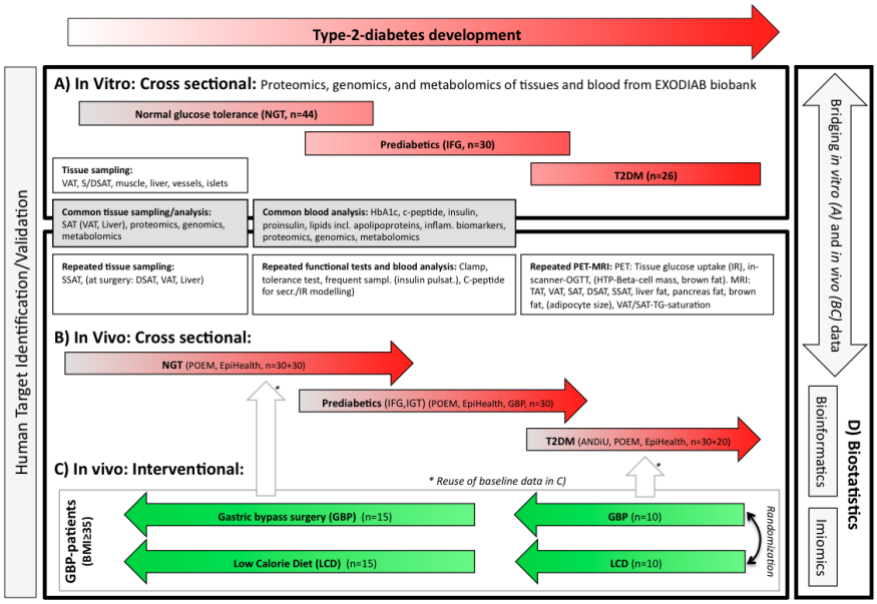

Figure 16. AstraZeneca, Uppsala University and SciLifeLab collaboration. Project overview. Figure from Prof. Håkan Ahlström.

Paper I-III involved both the *in vivo* and *in vitro* cross-sectional part of the study. **Paper I** was the first integrative effort undertaken to analyse whole-body imaging data with Imiomics and metabolomics. **Paper II** was an effort to utilise the complementary data acquired with three technologies, namely, PET, MRI and HEC, to accurately study whole-body glucose metabolism. The study involved significant feature engineering work as is further explained in **Chapter 9**. **Paper III** was primarily a method development effort with the aim to quickly be able to generate hypotheses from large amounts of Imiomics-generated 3D correlation maps. The effort was the result of an infrastructure change in our research group. As the Bianca HPC cluster was made accessible, generating voxel-wise correlation volumes at scale became feasible but presented increasing analysis challenges. The framework was designed to enable quick, intuitive and visual analysis of 3D Imiomics correlation maps without requiring the generation of complementary 3D p-value volumes. It was initially applied as a proof of concept on *cohort I* to explore the associations between clinical variables and tissue composition.

8.2 Cohort II

Cohort II is the result of continuous efforts in the UK Biobank study to collect extensive phenotypic and genotypic data from 500.000 participants (**Figure 17**)[129]. The UK Biobank is an outstanding resource for biomedical researchers, and it continues to accumulate massive amounts of open-access datasets. The UK Biobank MRI cohort represents one of the largest coherent imaging datasets available and presented a unique opportunity to explore Imiomics at scale[8]. The work presented in this thesis included the intersection of the imaging- and GWAS cohorts in the UK Biobank and was completed in collaboration with Professor Tove Fall's research group. To the best of our knowledge, **Paper IV** represents one of the largest body composition and imaging genetics studies to date. It required the integration of two massive and complex datasets for joint analysis and significant computational resources.

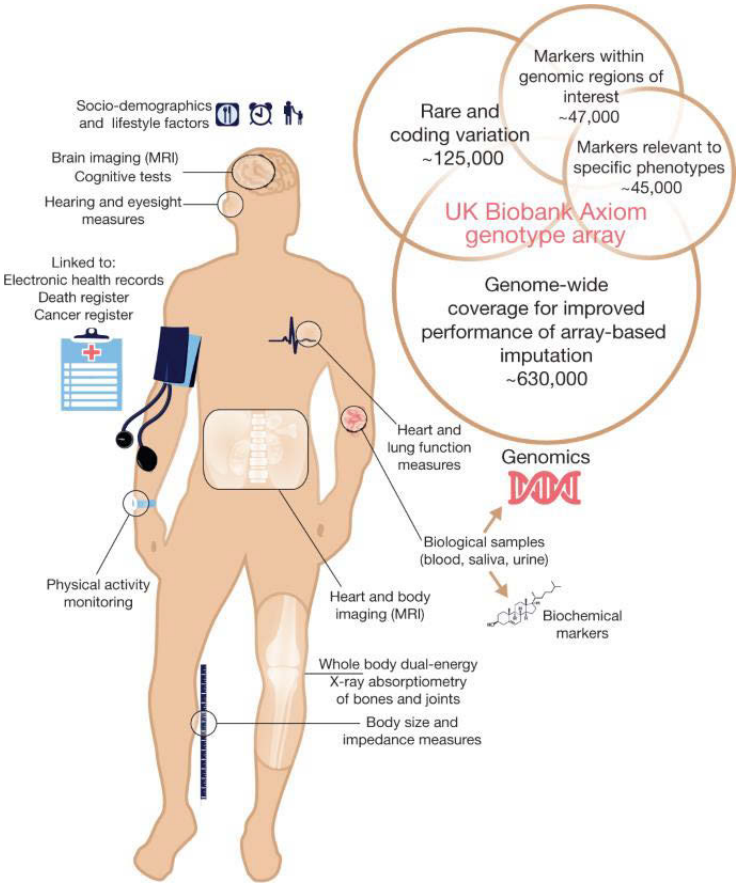

Figure 17. Schematic illustration of the extensive phenotypic- and genotypic data available in the UK Biobank. Reprint with CC BY 4.0. Bycroft et al. (2018).

9. Contributions

This is a comprehensive summary thesis based on the four papers summarised in this chapter.

9.1 Paper I

Integration of whole-body [18F]FDG PET/MRI with non-targeted metabolomics can provide new insights on tissue-specific insulin resistance in type 2 diabetes.

Klev Diamanti*, Robin Visvanathar*, Maria J. Pereira, Marco Cavalli, Gang Pan, Chanchal Kumar, Stanko Skrtic, Ulf Risérus, Jan W. Eriksson, Joel Kullberg, Jan Komorowski, Claes Wadelius and Håkan Ahlström.

Scientific Reports (2020).

Aims

To integrate whole-body imaging with non-targeted metabolomics and explore the associations between tissue-specific phenotypes and plasma/adipose tissue metabolites in healthy individuals and individuals with T2D.

Materials and Methods

This study was approved by the Regional Ethics Review Board in Uppsala (DNR 2014-313). Three groups of volunteers were included in the study, comprising of twelve healthy controls (6 female, 6 male) and sixteen individuals with prediabetes (9 female, 7 male) and fourteen individuals diagnosed with T2D (6 female, 8 male). Participants were matched for BMI, age and sex. Blood samples were collected following an overnight fast (>10h) for analyses of biomarkers and plasma metabolomics. SAT samples were retrieved for adipose tissue metabolomics analysis. The metabolomics analyses were performed using LC-MS and GC-MS at the Swedish Metabolomics Centre in Umeå, Sweden. Commercial and publicly available software were used for processing of the metabolomics data, including QC and targeted/untargeted compound identification. An integrated 3.0T PET/MR system (Signa PET/MR, GE Healthcare, Waukesha, WI) was used for image acquisition. Water- and adipose tissue separated images were used for further analyses following stepwise whole-body image registration with

Imiomics. Mann-Whitney U tests were used for differential analyses between groups, non-diabetes (ND, healthy volunteers + individuals with prediabetes) and T2D. The Benjamini-Hochberg procedure was used for multiple comparisons adjustment. Multiple regression models were used to study the associations between metabolites and body composition measurements. Statistical analyses were performed in RStudio (RStudio v.1.1.453, 2015) using custom scripts.

Results

A comprehensive mapping of the metabolome and tissue composition, including glucose uptake, was reported. 259 metabolites were identified in adipose tissue samples and 272 metabolites in plasma. BCAAs and AAAs were negatively associated with insulin sensitivity ($\beta = -0.25$, $p < 0.1$ and $\beta = -0.12$, $p < 0.1$, when pooled, respectively). Lysophosphatidylcholines (lysoPCs) in plasma were overrepresented in T2D compared with ND. Furthermore, of the plasma metabolites, lysoPC(P-16:0) was positively associated with SAT Ki ($\beta = 0.5$, $p < 0.1$) and inversely associated with hepatic fat content ($\beta = -0.62$, $p < 0.1$) (**Figure 18**).

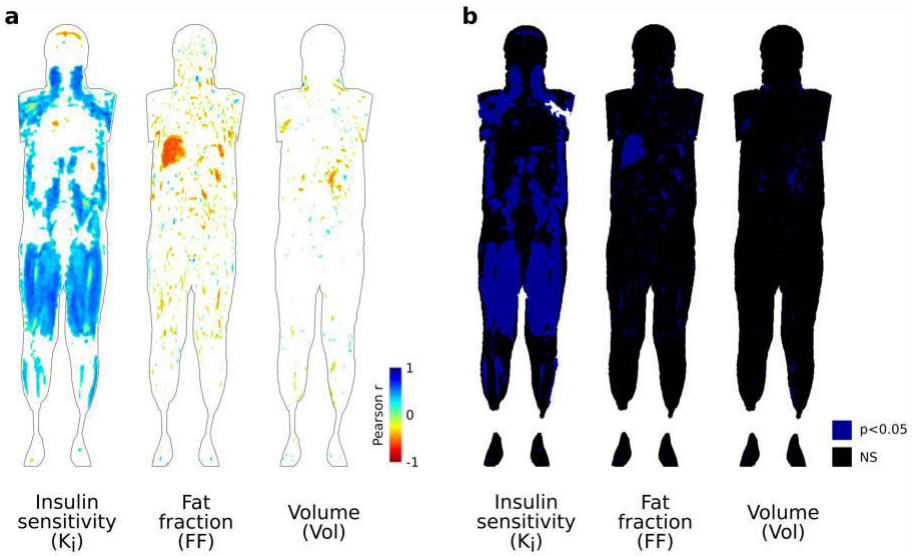

Figure 18: Voxel-level correlation maps between lysoPC(P-16:0) and tissue parameters generated with Imiomics. **a)** Pearson's r-coefficient maps showing only significant associations. **b)** P-value maps converted to masks ($p<0.05$), displaying only significant voxel-level associations.

Conclusion

Novel links between tissue composition and plasma/adipose tissue metabolites were presented. Systematic integration of whole-body imaging and non-targeted metabolomics is a powerful approach for exploratory "metabo-composition" research.

9.2 Paper II

Tissue-specific glucose partitioning and fat content in prediabetes and type 2 diabetes: whole-body PET/MRI during hyperinsulinemia.

Jan W. Eriksson, Robin Visvanathar, Joel Kullberg, Robin Strand, Stanko Skrtic, Simon Ekström, Mark Lubberink, Martin H. Lundqvist, Petros Katsogiannos, Maria J. Pereira and Håkan Ahlström.

European Journal of Endocrinology (2021).

Aims

To study whole-body glucose partitioning, tissue crosstalk and tissue-specific glucose uptake, volume and adipose tissue content in the development of T2D.

Materials and Methods

The study was approved by the Regional Ethics Review Board in Uppsala (DNR 2014-313). Three groups of volunteers were included in this study, comprising of twelve healthy controls (6 female, 6 male) and sixteen individuals with prediabetes (9 female, 7 male) and fourteen individuals diagnosed with T2D. Participants were matched for BMI, WHR, age and sex. Subjects were examined in the morning after overnight fasting and instructed to avoid alcohol and caffeine for a minimum of 6 hours prior to the examination, and to avoid intense physical activity 24 hours prior to the examination. The HEC was initiated with a priming dose, the insulin infusion rate was held constant at 56 mU/m^2 body surface/min. Simultaneously, a 20% glucose solution was infused at a variable rate to achieve a steady-state plasma glucose level of 5.6 mmol/L. When steady state was achieved, image acquisition was initiated. 4 MBq [^{18}F]FDG/kg bodyweight was injected intravenously with the initiation of a 10 min dynamic PET scan of the thorax to capture early tracer dynamics. This was followed by five whole-body PET scans (covering head to toe) and MR images generated for attenuation correction (MRAC) from a built-in dual-echo water-fat MRI sequence. Imiomics was used for image registration following the defined three-step process. Atlas-based image segmentation was performed for brain, heart, liver, VAT, SAT, gluteal-/thigh-/calf skeletal muscle.

Results

Several complex features were derived and studied, including endogenous glucose production.

$$EGP = R_D + V_{glu} + \frac{\Delta PG}{\Delta T} - GIR$$

$$R_D = \frac{(Dose_{FDG} + Urine_{FDG})}{AUC_{FDG}} \times SS_{glu}$$

We showed that impaired glucose uptake and metabolism during hyperinsulinemia in T2D is largely accounted for by skeletal muscle and to a lesser extent adipose tissue compartments and the liver. The relative contribution of skeletal muscle was 32% of whole-body Rd in participants with T2D vs 41% in healthy participants. Liver fat fraction was inversely associated with the glucose metabolic rate of all tissues except for the brain (**Figure 19**). Brain MR_{glu} was also positively associated with HbA1c and EGP. A gradually increasing proportion of whole-body glucose turnover during HEC was shown in the brains of individuals with T2D compared with prediabetes and healthy controls (7.1%, 5.5% and 3.8%, respectively).

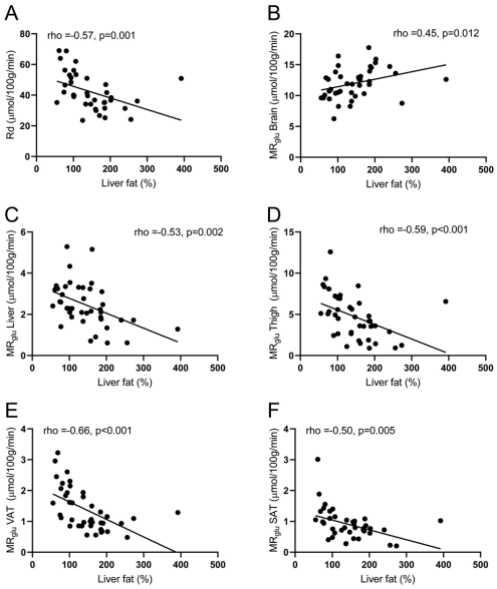

Figure 19. Scatter plots of significant bi-variate correlations. Liver fat % vs Rd (A), brain MRglu (B), liver MRglu (C), thigh MRglu (D), VAT MRglu (E) and SAT MRglu (F).

Conclusion

The use of integrated PET/MRI during HEC for studying detailed whole-body glucose turnover was demonstrated. Insulin-stimulated glucose partitioning and absolute glucose uptake rates in the brain were altered in individuals with T2D, revealing a potential key role of the brain in glucose homeostasis.

9.3 Paper III

Exploration of whole-body PET/MRI data and clinical variables in type 2 diabetes for data-driven hypothesis generation.

Robin Visvanathar, Lina Carlbom, Simon Ekström, Stanko Skrtic, Maria J. Pereira, Jan W. Eriksson, Håkan Ahlström and Joel Kullberg.

Manuscript.

Aims

To develop a rapid hypothesis-generating framework for the analysis of rich 3D correlation maps produced with Imiomics using whole-body PET/MRI and clinical variables in T2D.

Materials and Methods

The dataset used for method development of the hypothesis-generating framework overlaps with Paper I-II. Voxel-wise correlation maps were generated for 30 clinical biomarkers and PET/MR data. An optimized, distributed computational approach was developed and applied for statistical inference. The correlation maps were stratified based on three groups of effect sizes: weak, moderate and strong. Confidence intervals were estimated by using arctanh transformation on the generated effect size distributions.

Results

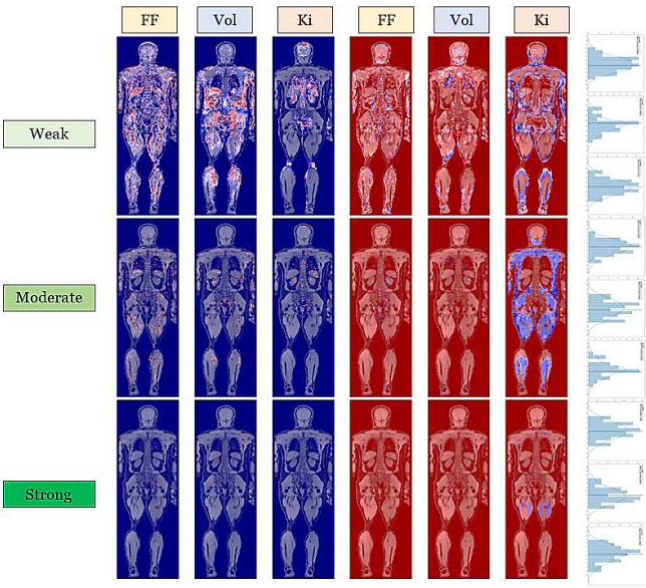

Figure 20. Stratified correlation maps generated for C-reactive protein (CRP). Blue background: positive associations, red background: negative associations. The correlation map illustrates a moderate inverse association between CRP and K_i in skeletal muscle.

P-CRP was positively associated with VAT volume but negatively associated with K_i in whole-body skeletal muscle. P-CRP was positively associated with fat fraction in the liver and skeletal muscle (**Figure 20**). In general, the same pattern was observed for other inflammatory biomarkers. There was a negative association between fat fraction in skeletal muscle and P-Creatinine. Conversely, P-Creatinine was positively associated with fat fraction around the kidneys. Whole-body insulin sensitivity, the M-value, was positively associated with skeletal muscle glucose uptake, but inversely associated with glucose uptake in the brain.

Conclusion
A data-driven hypothesis-generating analysis method for quick, intuitive and visual analysis of 3D correlation maps produced with Imiomics was developed. The method enables effortless identification of non-imaging data associations from volumetric maps.

9.4 Paper IV

Genetic variation and sex-stratified advanced body composition analysis: neck-to-knee MRI and genetics in the UK Biobank.
Robin Visvanathar, Jenny Censin, Uwe Menzel, Shafqat Ahmad, Filip Malmberg, Joel Kullberg, Tove Fall and Håkan Ahlström.
Manuscript.

Aims
To integrate Imiomics with GWAS and explore sex-stratified imaging genetics for the discovery of novel links between genetic variation and body composition in the UK Biobank.

Materials and Methods
A total of 27,149 participants (13,300 men and 13,849 women) were included after GWAS and imaging QC (**Figure 21**). A dual-echo Dixon imaging protocol was used for the acquisition of water- and fat separated MR images. Images were acquired on a 1.5T Siemens Aera MR system using the following scan parameters: TE=2.39/4.77ms, TR=6.69, α=10° and voxel size=2.232^2x3mm^3. Mean intensity projections of the volumetric MRI data were visually assessed and checked for water-fat swaps, high background noise or corrupted data. A three-step image registration process was completed to deform all volumetric data to a common coordinate system. Four imaging subgroups (male/female, tissue volume/fat fraction) were used for advanced body composition analysis with Imiomics. Sex-stratified Pearson correlation coefficient maps were calculated for all subgroups to study the relationship between body composition and risk scores for BMI, WHR and

height. Six selected SNPs were further included for detailed mapping to body composition with Imiomics. Tissue segmentations of VAT, abdominal SAT, gluteofemoral SAT, heart, liver and thigh muscle were used for quantification and comparison within and between groups.

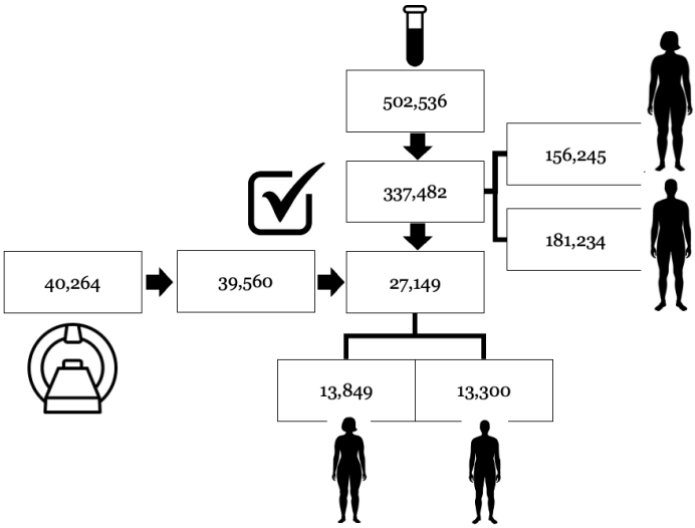

Figure 21. Schematic overview of participant selection. A total of 27,194 participants were included in the study following GWAS- and imaging quality control.

Results

Imiomics and GWAS integration delivered a detailed mapping of individual SNPs with the tissue composition of regional adipose tissue depots, heart, liver, lungs and thigh muscle (**Figure 22**).

In both sexes, the rs1358980-T variant was the highest ranked SNP inversely associated with gluteofemoral SAT volume (**Figure 23**). In men, rs1358980 was positively associated with VAT fat fraction ($r = 0.039$, $p<0.05$) and heart fat fraction ($r = 0.004$, <0.05). Rs1358980 was also the SNP with the strongest inverse association with gluteofemoral SAT fat fraction in men ($r = -0.007$, $p<0.05$). Top ranked SNPs that were positively associated with all tissue volumes were rs6567160 and rs13021737 for both men and women. In women, rs6567160 was positively associated with liver fat fraction ($r = 0.0056$, $p<0.05$) and thigh fat fraction ($r = 0.0052$, $p<0.05$), but inversely associated with gluteofemoral SAT fat fraction ($r = -0.0058$, $p<0.05$), The same inverse trend between rs6567160 and gluteofemoral SAT fat fraction was observed in men. Several additional novel tissue composition and SNP relationships were found. For the genetic risk scores, observed effect sizes were higher with LDpred-derived PRS compared with genome-wide significant only scores.

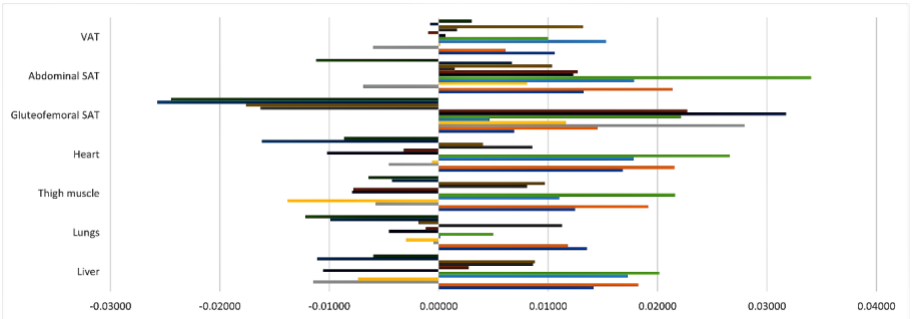

	Liver	Lungs	Thigh muscle	Heart	Gluteofemoral SAT	Abdominal SAT	VAT
M rs1358980	-0.00597	-0.01221	-0.00639	-0.00865	-0.02445	-0.01119	0.00301
F rs1358980	-0.01113	-0.00991	-0.00427	-0.01614	-0.02574	0.00671	-0.00078
M rs1936805	0.00878	-0.00183	0.00969	0.00407	-0.01761	0.01037	0.01318
F rs1936805	0.00863	0.01129	0.00809	0.00855	-0.01630	0.00147	0.00166
M rs2820443	0.00275	-0.00116	-0.00781	-0.00319	0.02273	0.01273	-0.00098
F rs2820443	-0.01054	-0.00456	-0.00792	-0.01019	0.03175	0.01232	0.00063
M rs6567160	0.02018	0.00499	0.02162	0.02663	0.02215	0.03402	0.01001
F rs6567160	0.01725	0.00015	0.01104	0.01783	0.00466	0.01786	0.01532
M rs10195252	-0.00735	-0.00296	-0.01380	-0.00061	0.01163	0.00807	0.00014
F rs10195252	-0.01147	-0.00045	-0.00573	-0.00455	0.02795	-0.00690	-0.00600
M rs13021737	0.01826	0.01180	0.01914	0.02157	0.01449	0.02135	0.00608
F rs13021737	0.01413	0.01357	0.01247	0.01683	0.00691	0.01325	0.01061

Figure 22. Associations between all SNPs and tissue-specific volumes in men and women. The raw data for all 84 associations is displayed below the graph. Abbreviations: Male (M), Female (F), Subcutaneous adipose tissue (SAT), Visceral adipose tissue (VAT).

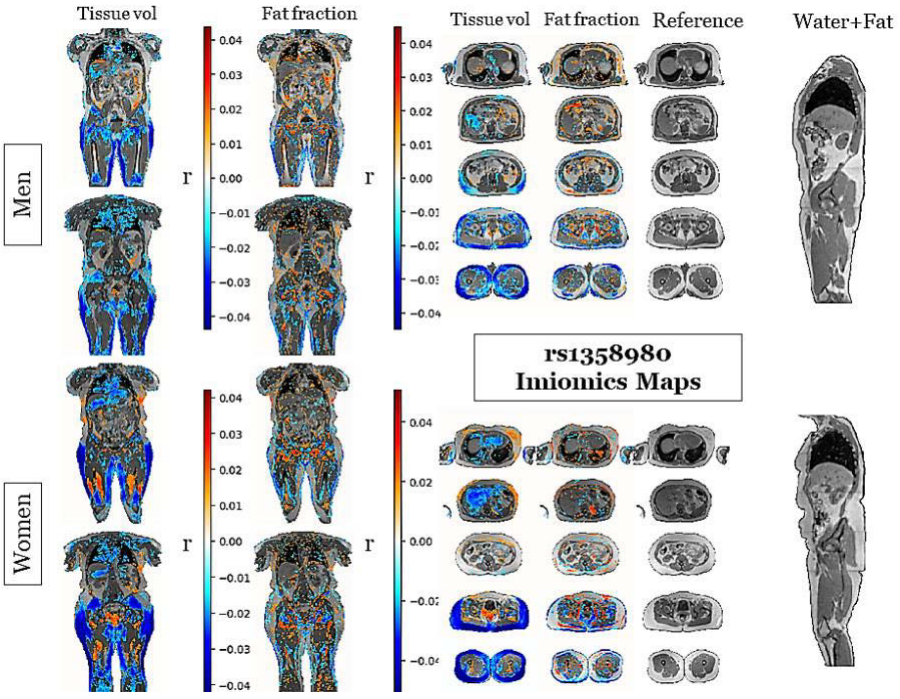

Figure 23. Illustrative visualisation of Imiomics outputs. Sex-stratified voxel-wise correlation maps of rs1358980 with tissue volumes and fat fraction are shown. Rs1358980 is inversely associated with the volume of gluteofemoral SAT in both sexes. The colorbars represents the Pearson correlation coefficient (r), only statistically significant ($p<0.05$) voxels are shown in colour.

Conclusion

Imiomics and GWAS were successfully combined to generate a mapping between genetics and imaging-derived features. Novel links between SNPs and detailed body composition features were reported. To the best of our knowledge, this is one of the largest advanced body composition and imaging genetics studies to date.

10. Discussion

The work discussed in this thesis represents a multidisciplinary effort to integrate complex datasets by leveraging an image-based approach. Imiomics-guided advanced body composition analysis when combined with orthogonal data sources, either through multimodal imaging and HEC or -omics techniques, could discover original multi-layered results. In the following passages, I will attempt to describe the lessons that have originated from the repeated application of image-based methods, primarily Imiomics, to study complex body composition relationships.

10.1 Complicated study of glucose metabolism

The complementary strengths of ^{18}F-FDG PET and MR data were illustrated in **Paper II**. The combined modalities together with HEC allowed us to perform detailed quantification of whole-body glucose turnover. In terms of lessons, the study highlighted the difficult balance of working with complex imaging features and the circularity of limited sample sizes because of the complicated acquisition protocols required to capture those complex imaging features. To exemplify, in the study an initial short dynamic PET scan was performed to capture early tracer dynamics which was required for the image-derived input function (IDIF)[34]. The IDIF replaced serial arterial blood sampling that would otherwise be preferred to measure radioactivity concentrations in the plasma[130]. Ultimately, the IDIF was used to estimate ^{18}F-FDG uptake rate or the net influx parameter, K_i. The ^{18}F-FDG uptake rate was further transformed to MR_{glu} (the glucose metabolic rate per 100g tissue) with the help of steady state glucose levels from HEC. MR_{glu} was further propagated for additional feature engineering to leverage the three modalities fully, this is schematically illustrated in **Figure 24**.

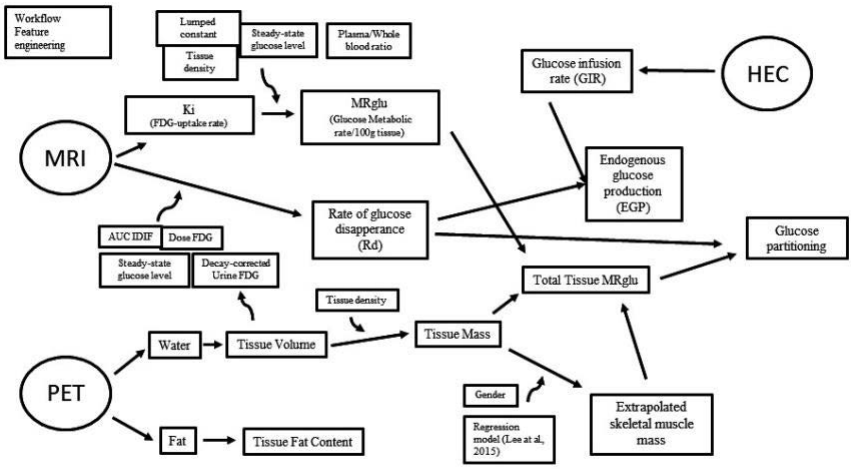

Figure 24. The complex feature engineering in Paper II. Integration of PET, MRI and HEC data.

The caveat was that with more complex imaging features, assumptions and minor inherent variances were compounded, and statistically grounded conclusions made less likely. Furthermore, due to the complex nature of the acquisition protocols sample size could not be significantly increased to compensate for the added complexity. The primary finding of the study was the observation of altered glucose metabolism in the brain during T2D development, however, it is likely that we missed several relevant and important findings due to the compounded noise in the complex features. This was evident by the many near-significant results in the study and emphasised the challenge of integrating whole-body multimodal data for detailed glucose metabolism studies.

10.2 The challenges of -omics

The first ever Imiomics and metabolomics study was performed in **paper I**. Differential analysis in ND and T2D revealed differences in metabolite composition that were further investigated with Imiomics. The combination of two inherently exploratory approaches, namely untargeted metabolomics and Imiomics, presented significant interpretation challenges with respect to statistics and the biological relevance of the findings. This was reinforced by the nature of the dataset, being of limited sample size yet massively high-dimensional. The same lessons were reflected upon in **paper IV**, where the first ever Imiomics and genomics study was performed. Although the significantly increased sample size in **paper IV** mitigated the typical statistical weaknesses of an exploratory study, there were remaining challenges with

respect to the interpretation of the generous outputs. Typical -omics studies including genomics, metabolomics, proteomics, transcriptomics and Imiomics, output massive amounts of results in accordance with their high-throughput distinguishing feature. For the Imiomics-based -omics integration studies in **paper I and IV**, the most challenging part was the interpretation of bivariate correlations between imaging-derived features and metabolites or genetic variants. *Correlation does not imply causation* hence even statistically significant associations become difficult to contextualise when studying links between alterations on the molecular biology level and body composition phenotypes. Ultimately, the additional orthogonal validation from the literature provided enough support to discover novel insights in **paper I and IV**. Nevertheless, one suggestion for future research with Imiomics is to step away from correlation maps towards more advanced statistical inference modelling e.g., mendelian randomisation with Imiomics to explore image-based causality analysis. The method development work conducted in this thesis could support such progress, specifically enabling voxel-wise statistical inference on a distributed system for orders of magnitude more efficient computation.

10.3 Holistic analysis of volumetric Imiomics maps

There were a total of 12,568,640 voxels in a typical volumetric image, which meant 12,568,640 statistical tests were performed every time an Imiomics map was created. Multiple testing correction using the traditional Bonferroni method in most cases would demolish any significant findings. There are various ways to address this challenge i.e., downsampling for dimensionality reduction, pre-segmentation to remove irrelevant voxels or using a different multiple comparison correction method. They all have different strengths and weaknesses, downsampling comes with the risk of removing relevant details, and attempting to mask out background could make the process more complicated and less efficient. Different multiple comparison methods for voxel-wise statistics were evaluated recently by Breznik et al.[105]. The conclusion was that permutation-based approaches would be most appropriate, but they are computationally demanding. Still, in **paper IV** a permutation-based correction method was used but the number of iterations was in the 100s and not the typical 1000s.

Paper III aimed to develop a method for the study of Imiomics maps without p-values. The method intended to leverage the effect size and sample size to estimate confidence in findings by using the Fisher z-transformation. The volumetric maps were analysed with stratified visualisations according to an old system introduced by the prominent statistician Jacob Cohen in 1988[131]. As a proof-of-concept the method was applied to study the associations between clinical variables and body composition. However, it is worth mentioning that the same system likely will not work with Imiomics-guided

genomics and metabolomics studies. The effect sizes in those studies are simply too small, in future developments one could step away from Cohen's definitions and instead stratify visualisations and findings based on relative observed effect sizes. Furthermore, incorporating projection-based visualisations e.g., mean- or median intensity projections, could potentially reduce tedious analysis hours and simplify the workflow.

Statistical rigor is an interesting topic in the era of -omics studies. Arguably, there is a degree of overreliance on the predetermined notion of statistical significance in the medical research community, and too little emphasis on descriptive statistics for inferring biological relevance. I will leave it to the reader to interpret the words of Sir Ronald Aylmer Fisher, one of the most ground-breaking modern statisticians in history[132].

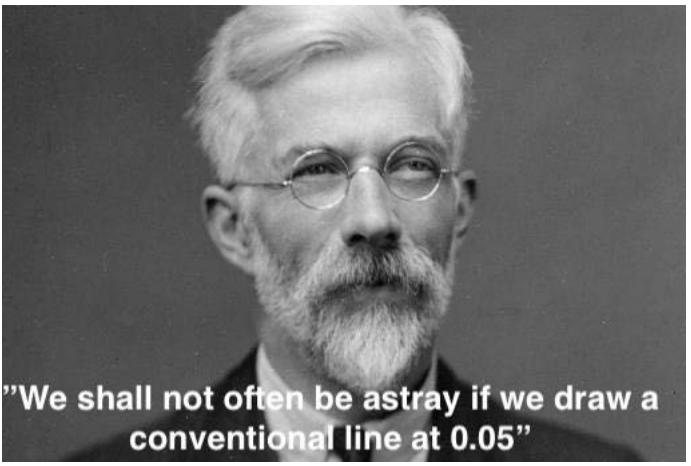

10.4 Conclusions and future perspectives

Imiomics is an innovative and original analysis framework intended for applied, large-scale and interdisciplinary body composition research. The results presented in this thesis has contributed to the methodological development of Imiomics and further demonstrated the utility of Imiomics in combination with metabolomics and genomics, respectively. **Paper I** describes the integration of whole-body imaging with metabolomics to reveal novel metabolite-phenotype associations in T2D. **Paper II** describes the accurate study of glucose turnover in T2D by combining whole-body PET/MRI and HEC. **Paper III** describes a hypothesis-generating framework for scalable analysis of large amounts of 3D Imiomics maps. **Paper IV** describes the integration of Imiomics with GWAS to explore heritability and body composition.

Most -omics technologies experience two initial stages of development in the research community. The first stage is generally characterised by high

costs, hints of scalability, limited utility and significant method development on both the hardware and software side. The second stage is characterised by increased utility, scalability, low costs, increased accessibility and consequently significant software method development. The work discussed in this thesis represents the early transition phase of Imiomics, where scalability, increased utility and software development have been in focus. Importantly, there is still a long way to go before Imiomics becomes a mainstream technology like other -omics platforms. Barriers include significant hardware costs, demands on computational resources and interdisciplinary efforts to pave the way for innovation. Navigating the transition from hypothesis-driven high utility studies, in the traditional research community, to exploratory hypothesis-generating low utility studies, is a major challenge for all -omics technologies. Fortunately, large open-access biobanks such as the UK Biobank provides tremendous potential for innovation. This thesis illustrates an important concept as we move forward i.e., the increased utility achieved by integrating orthogonal datasets to further support novel insights.

Populärvetenskaplig sammanfattning

I denna avhandling presenteras fyra arbeten där kroppsammansättning har studerats i detalj med hjälp av magnetisk resonanstomografi (MRT) och metabolism med positronemissionstomografi (PET). Det övergripande målet var att bidra till forskning som berör kroppsammansättning och bildanalys. Det innovativa bildanalys konceptet, Imiomics, applicerades och vidareutvecklades för att möjliggöra nya applikationer.

Delarbete I

I detta delarbete användes Imiomics tillsammans med metabolomics för att studera relationen mellan kroppssammansättning och ämnesomsättning i typ-2 diabetes. Vävnadsvolymer och fetthalter analyserades i relation till metaboliter i plasma och fettväv. Flera nya och erkända fynd presenterades såsom relationer mellan fosfolipider och aminosyror med leverns fetthalt. Ett flertal metaboliter som skiljde sig åt mellan friska individer och individer med typ-2 diabetes rapporterades. Detta var den första studien där helkroppsbildanalys med Imiomics kunde kombineras med metabolomics.

Delarbete II

I detta delarbete användes PET och MRT (PET/MR) för att studera olika vävnaders glukosupptag till följd av insulinstimulering. Det totala glukosupptaget i kroppen och relativa glukosupptaget i vävnader jämfördes mellan friska individer och individer med typ-2 diabetes. Hjärnans glukosupptag i individer med typ-2 diabetes var förhöjt jämfört friska individer, och levern fetthalt var associerad med andra vävnaders glukosupptag.

Delarbete III

I detta delarbete utvecklades en enkel metod för att analysera Imiomics bilder. Metoden applicerades på MR och PET data för att studera relationen mellan vardagliga kliniska variabler och vävnadskomposition. Metoden var baserad på statistiska genvägar för att undvika beräkningsintensiva steg med Imiomics och ämnade att förenkla analys av stora mängder Imiomics data.

Delarbete IV

I detta delarbete användes Imiomics på helkropps-MR tillsammans med genomics för att studera hur genetisk variation påverkar

kroppssammansättning. Detaljerade vävnadskartor av relationen mellan specifika enbaspolymorfier (*eng.* SNPs) och vävnadsvolym samt fetthalt presenterades. Studien inkluderade över 20,000 individer och var den första studien där helkroppsbildanalys med Imiomics kunde kombineras med genomics.

Sammantaget har delarbetena bidragit till forskning om kroppsammansättning genom applicerad bildanalys, med fokus på Imiomics tillsammans med flera oberoende teknologier som metabolomics och genomics.

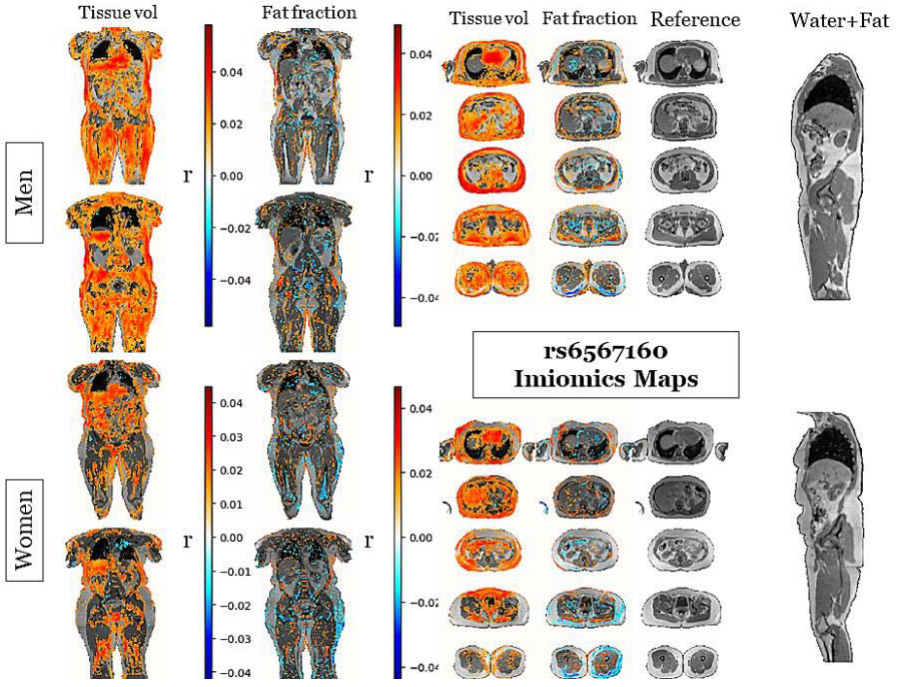

Exempel på korrelationskartor skapade med Imiomics.

Acknowledgements

I am inclined to believe that it is extremely difficult to find a perfect PhD supervisor, that is why I am incredibly grateful to my main supervisor, **Håkan Ahlström**. I appreciate the genuine friendship, guidance, inspiration, jokes, feedback, many lunches and philosophical discussions that we have had during these last few years and hopefully will continue to have for many more years.

I would also like to acknowledge my co-supervisors, **Joel Kullberg** and **Jan W. Eriksson**, for sharing their passion for research, insights and support.

My colleagues and friends from our research group, **Therese Sjöholm, Elin Lundström, Jonathan Andersson, Simon Ekström, Taro Langner, Filip Malmberg, Robin Strand, Hanna Jönsson, Brent Sanchez and Andrés Martínez Mora,** thank you all for your friendship and kindness.

I am thankful to all of the people that I have had the privilege to collaborate with, a special thanks to **Maria J. Pereira, Klev Diamanti and Jenny Censin** for rewarding and great teamwork.

I am also immensely grateful to the people that introduced me to research, **Samer Siwani, Sanja Mikulovic and Angelica Thulin**, rarely have I come across such amazing individuals and friends.

I have had the privilege to work with many individuals during these last few years, thank you to all of you – friends, colleagues and mentors.

References

1. The human body at cellular resolution: the NIH Human Biomolecular Atlas Program. *Nature* **574**, 187–192 (2019).
2. Manzoni, C. *et al.* Genome, transcriptome and proteome: the rise of omics data and their integration in biomedical sciences. *Brief. Bioinform.* **19**, 286–302 (2018).
3. Hemke, R., Buckless, C. & Torriani, M. Quantitative Imaging of Body Composition. *Semin. Musculoskelet. Radiol.* **24**, 375–385 (2020).
4. Higgins, M. I., Marquardt, J. P., Master, V. A., Fintelmann, F. J. & Psutka, S. P. Machine Learning in Body Composition Analysis. *Eur. Urol. Focus* **7**, 713–716 (2021).
5. Lee, B. J. & Yim, M. H. Comparison of anthropometric and body composition indices in the identification of metabolic risk factors. *Sci. Rep.* **11**, 9931 (2021).
6. Lemos, T. & Gallagher, D. Current body composition measurement techniques. *Curr. Opin. Endocrinol. Diabetes Obes.* **24**, 310–314 (2017).
7. Borga, M. *et al.* Advanced body composition assessment: from body mass index to body composition profiling. *J. Investig. Med.* **66**, 1–9 (2018).
8. Littlejohns, T. J. *et al.* The UK Biobank imaging enhancement of 100,000 participants: rationale, data collection, management and future directions. *Nat. Commun.* **11**, 2624 (2020).
9. Wichmann, H.-E., Hörlein, A., Ahrens, W. & Nauck, M. [The biobank of the German National Cohort as a resource for epidemiologic research]. *Bundesgesundheitsblatt Gesundheitsforschung Gesundheitsschutz* **59**, 351–360 (2016).
10. Linge, J., Petersson, M., Forsgren, M. F., Sanyal, A. J. & Dahlqvist Leinhard, O. Adverse muscle composition predicts all-cause mortality in the UK Biobank imaging study. *J. Cachexia Sarcopenia Muscle* **12**, 1513–1526 (2021).
11. Christakoudi, S., Tsilidis, K. K., Evangelou, E. & Riboli, E. Association of body-shape phenotypes with imaging measures of body composition in the UK Biobank cohort: relevance to colon cancer risk. *BMC Cancer* **21**, 1106 (2021).
12. Bland, V. L. *et al.* Cross-sectional associations between adipose tissue depots and areal bone mineral density in the UK Biobank imaging study. *Osteoporos. Int.* **33**, 391–402 (2022).
13. Livingstone, K. M. *et al.* Discovery Genome-Wide Association Study of Body Composition in 4,386 Adults From the UK Biobank's Pilot Imaging Enhancement Study. *Front. Endocrinol.* **12**, (2021).
14. Karastergiou, K., Smith, S. R., Greenberg, A. S. & Fried, S. K. Sex differences in human adipose tissues – the biology of pear shape. *Biol. Sex Differ.* **3**, 13 (2012).
15. Bredella, M. A. Sex Differences in Body Composition. in *Sex and Gender Factors Affecting Metabolic Homeostasis, Diabetes and Obesity* (ed. Mauvais-Jarvis, F.) vol. 1043 9–27 (Springer International Publishing, 2017).

16. Manolopoulos, K. N., Karpe, F. & Frayn, K. N. Gluteofemoral body fat as a determinant of metabolic health. *Int. J. Obes.* **34**, 949–959 (2010).
17. Snijder, M. B. *et al.* Low subcutaneous thigh fat is a risk factor for unfavourable glucose and lipid levels, independently of high abdominal fat. The Health ABC Study. *Diabetologia* **48**, 301–308 (2005).
18. Bjørndal, B., Burri, L., Staalesen, V., Skorve, J. & Berge, R. K. Different Adipose Depots: Their Role in the Development of Metabolic Syndrome and Mitochondrial Response to Hypolipidemic Agents. *J. Obes.* **2011**, e490650 (2011).
19. Wang, H. & Eckel, R. H. Lipoprotein lipase: from gene to obesity. *Am. J. Physiol.-Endocrinol. Metab.* **297**, E271–E288 (2009).
20. Nielsen, T. S., Jessen, N., Jørgensen, J. O. L., Møller, N. & Lund, S. Dissecting adipose tissue lipolysis: molecular regulation and implications for metabolic disease. *J. Mol. Endocrinol.* **52**, R199–R222 (2014).
21. Luders, E., Gaser, C., Narr, K. L. & Toga, A. W. Why Sex Matters: Brain Size Independent Differences in Gray Matter Distributions between Men and Women. *J. Neurosci.* **29**, 14265–14270 (2009).
22. Janssen, I., Heymsfield, S. B., Wang, Z. & Ross, R. Skeletal muscle mass and distribution in 468 men and women aged 18–88 yr. *J. Appl. Physiol.* **89**, 81–88 (2000).
23. Godoy, I. R. B. *et al.* Fat accumulation in the tongue is associated with male gender, abnormal upper airway measures and whole-body adiposity. *Metabolism.* **65**, 1657–1663 (2016).
24. Braun, S., Bitton-Worms, K. & LeRoith, D. The Link between the Metabolic Syndrome and Cancer. *Int. J. Biol. Sci.* **7**, 1003–1015 (2011).
25. Grundy, S. M. Obesity, Metabolic Syndrome, and Cardiovascular Disease. *J. Clin. Endocrinol. Metab.* **89**, 2595–2600 (2004).
26. Sutherland, J. P., McKinley, B. & Eckel, R. H. The Metabolic Syndrome and Inflammation. *Metab. Syndr. Relat. Disord.* **2**, 82–104 (2004).
27. Khan, M. A. B. *et al.* Epidemiology of Type 2 Diabetes – Global Burden of Disease and Forecasted Trends. *J. Epidemiol. Glob. Health* **10**, 107–111 (2020).
28. Zhou, B. *et al.* Worldwide trends in diabetes since 1980: a pooled analysis of 751 population-based studies with 4·4 million participants. *The Lancet* **387**, 1513–1530 (2016).
29. American Diabetes Association. 2. Classification and Diagnosis of Diabetes: Standards of Medical Care in Diabetes—2021. *Diabetes Care* **44**, S15–S33 (2020).
30. Eyth, E. & Naik, R. Hemoglobin A1C. in *StatPearls* (StatPearls Publishing, 2022).
31. Wallace, T. M., Levy, J. C. & Matthews, D. R. Use and Abuse of HOMA Modeling. *Diabetes Care* **27**, 1487–1495 (2004).
32. Jagannathan, R. *et al.* The Oral Glucose Tolerance Test: 100 Years Later. *Diabetes Metab. Syndr. Obes. Targets Ther.* **13**, 3787–3805 (2020).
33. Kim, J. K. Hyperinsulinemic-euglycemic clamp to assess insulin sensitivity in vivo. *Methods Mol. Biol. Clifton NJ* **560**, 221–238 (2009).
34. Johansson, E. *et al.* Whole-Body Imaging of Tissue-specific Insulin Sensitivity and Body Composition by Using an Integrated PET/MR System: A Feasibility Study. *Radiology* **286**, 271–278 (2018).
35. Sneed, N. M. & Morrison, S. A. Body Composition Methods in Adults with Type 2 Diabetes or at Risk for T2D: a Clinical Review. *Curr. Diab. Rep.* **21**, 14 (2021).

36. Cobb, M. 60 years ago, Francis Crick changed the logic of biology. *PLoS Biol.* **15**, e2003243 (2017).
37. Crick, F. H. C. ON PROTEIN SYNTHESIS. *Mol. Biol.* 27 (1956).
38. Przybyla, L. & Gilbert, L. A. A new era in functional genomics screens. *Nat. Rev. Genet.* **23**, 89–103 (2022).
39. Verlouw, J. A. M. *et al.* A comparison of genotyping arrays. *Eur. J. Hum. Genet.* **29**, 1611–1624 (2021).
40. Uffelmann, E. *et al.* Genome-wide association studies. *Nat. Rev. Methods Primer* **1**, 1–21 (2021).
41. Hu, Y. J. & Lin, D. Y. Analysis of Untyped SNPs: Maximum Likelihood and Imputation Methods. *Genet. Epidemiol.* **34**, 803–815 (2010).
42. Hirschhorn, J. N. & Gajdos, Z. K. Z. Genome-Wide Association Studies: Results from the First Few Years and Potential Implications for Clinical Medicine. *Annu. Rev. Med.* **62**, 11–24 (2011).
43. Klein, R. J. *et al.* Complement factor H polymorphism in age-related macular degeneration. *Science* **308**, 385–389 (2005).
44. Visscher, P. M. *et al.* 10 Years of GWAS Discovery: Biology, Function, and Translation. *Am. J. Hum. Genet.* **101**, 5–22 (2017).
45. Morris, A. P. *et al.* Large-scale association analysis provides insights into the genetic architecture and pathophysiology of type 2 diabetes. *Nat. Genet.* **44**, 981–990 (2012).
46. Xue, A. *et al.* Genome-wide association analyses identify 143 risk variants and putative regulatory mechanisms for type 2 diabetes. *Nat. Commun.* **9**, 2941 (2018).
47. Franke, A. *et al.* Genome-wide meta-analysis increases to 71 the number of confirmed Crohn's disease susceptibility loci. *Nat. Genet.* **42**, 1118–1125 (2010).
48. Barrett, J. C. *et al.* Genome-wide association defines more than 30 distinct susceptibility loci for Crohn's disease. *Nat. Genet.* **40**, 955–962 (2008).
49. Stahl, E. A. *et al.* Genome-wide association study meta-analysis identifies seven new rheumatoid arthritis risk loci. *Nat. Genet.* **42**, 508–514 (2010).
50. Sandhu, M. S. *et al.* LDL-cholesterol concentrations: a genome-wide association study. *Lancet* **371**, 483–491 (2008).
51. Richards, J. B., Zheng, H.-F. & Spector, T. D. Genetics of osteoporosis from genome-wide association studies: advances and challenges. *Nat. Rev. Genet.* **13**, 576–588 (2012).
52. Frayling, T. M. *et al.* A common variant in the FTO gene is associated with body mass index and predisposes to childhood and adult obesity. *Science* **316**, 889–894 (2007).
53. Scuteri, A. *et al.* Genome-Wide Association Scan Shows Genetic Variants in the FTO Gene Are Associated with Obesity-Related Traits. *PLoS Genet.* **3**, e115 (2007).
54. Tam, V. *et al.* Benefits and limitations of genome-wide association studies. *Nat. Rev. Genet.* **20**, 467–484 (2019).
55. Goldstein, D. B. Common Genetic Variation and Human Traits. *N. Engl. J. Med.* **360**, 1696–1698 (2009).
56. McClellan, J. & King, M.-C. Genetic Heterogeneity in Human Disease. *Cell* **141**, 210–217 (2010).
57. Manolio, T. A. *et al.* Finding the missing heritability of complex diseases. *Nature* **461**, 747–753 (2009).
58. McCarthy, M. I. *et al.* Genome-wide association studies for complex traits: consensus, uncertainty and challenges. *Nat. Rev. Genet.* **9**, 356–369 (2008).

59. Collister, J. A., Liu, X. & Clifton, L. Calculating Polygenic Risk Scores (PRS) in UK Biobank: A Practical Guide for Epidemiologists. *Front. Genet.* **13**, (2022).
60. Janssens, A. C. J. & van Duijn, C. M. Genome-based prediction of common diseases: methodological considerations for future research. *Genome Med.* **1**, 20 (2009).
61. Liu, X. & Locasale, J. W. Metabolomics: A Primer. *Trends Biochem. Sci.* **42**, 274–284 (2017).
62. Zeki, Ö. C., Eylem, C. C., Reçber, T., Kır, S. & Nemutlu, E. Integration of GC–MS and LC–MS for untargeted metabolomics profiling. *J. Pharm. Biomed. Anal.* **190**, 113509 (2020).
63. Alseekh, S. *et al.* Mass spectrometry-based metabolomics: a guide for annotation, quantification and best reporting practices. *Nat. Methods* **18**, 747–756 (2021).
64. Pitt, J. J. Principles and Applications of Liquid Chromatography-Mass Spectrometry in Clinical Biochemistry. *Clin. Biochem. Rev.* **30**, 19–34 (2009).
65. Misra, B. B. New software tools, databases, and resources in metabolomics: updates from 2020. *Metabolomics Off. J. Metabolomic Soc.* **17**, 49 (2021).
66. Xiao, J. F., Zhou, B. & Ressom, H. W. Metabolite identification and quantitation in LC-MS/MS-based metabolomics. *Trends Anal. Chem. TRAC* **32**, 1–14 (2012).
67. Wishart, D. S. *et al.* HMDB 5.0: the Human Metabolome Database for 2022. *Nucleic Acids Res.* **50**, D622–D631 (2022).
68. Chen, Z.-Z. & Gerszten, R. E. Metabolomics and Proteomics in Type 2 Diabetes. *Circ. Res.* **126**, 1613–1627 (2020).
69. Fall, T. *et al.* Non-targeted metabolomics combined with genetic analyses identifies bile acid synthesis and phospholipid metabolism as being associated with incident type 2 diabetes. *Diabetologia* **59**, 2114–2124 (2016).
70. Würtz, P. *et al.* Branched-Chain and Aromatic Amino Acids Are Predictors of Insulin Resistance in Young Adults. *Diabetes Care* **36**, 648–655 (2013).
71. Wang, T. J. *et al.* Metabolite profiles and the risk of developing diabetes. *Nat. Med.* **17**, 448–453 (2011).
72. Drogan, D. *et al.* Untargeted Metabolic Profiling Identifies Altered Serum Metabolites of Type 2 Diabetes Mellitus in a Prospective, Nested Case Control Study. *Clin. Chem.* **61**, 487–497 (2015).
73. Liu, J. *et al.* Metabolomics based markers predict type 2 diabetes in a 14-year follow-up study. *Metabolomics* **13**, 104 (2017).
74. The Multiple Tissue Human Expression Resource (MuTHER) Consortium *et al.* An atlas of genetic influences on human blood metabolites. *Nat. Genet.* **46**, 543–550 (2014).
75. Hsu, Y.-H. H. *et al.* Integrating untargeted metabolomics, genetically informed causal inference, and pathway enrichment to define the obesity metabolome. *Int. J. Obes.* **44**, 1596–1606 (2020).
76. Liesenfeld, D. B. *et al.* Metabolomics and transcriptomics identify pathway differences between visceral and subcutaneous adipose tissue in colorectal cancer patients: the ColoCare study. *Am. J. Clin. Nutr.* **102**, 433–443 (2015).
77. Pinu, F. R. *et al.* Systems Biology and Multi-Omics Integration: Viewpoints from the Metabolomics Research Community. *Metabolites* **9**, 76 (2019).
78. Kastenmüller, G., Raffler, J., Gieger, C. & Suhre, K. Genetics of human metabolism: an update. *Hum. Mol. Genet.* **24**, R93–R101 (2015).
79. Kettunen, J. *et al.* Genome-wide study for circulating metabolites identifies 62 loci and reveals novel systemic effects of LPA. *Nat. Commun.* **7**, 11122 (2016).

80. Draisma, H. H. M. *et al.* Genome-wide association study identifies novel genetic variants contributing to variation in blood metabolite levels. *Nat. Commun.* **6**, 7208 (2015).
81. Tukiainen, T. *et al.* Detailed metabolic and genetic characterization reveals new associations for 30 known lipid loci. *Hum. Mol. Genet.* **21**, 1444–1455 (2012).
82. Shampo, M. A., Kyle, R. A. & Steensma, D. P. Richard Ernst—Nobel Prize for Nuclear Magnetic Resonance Spectroscopy. *Mayo Clin. Proc.* **87**, e109 (2012).
83. Chan, R. W., Lau, J. Y. C., Lam, W. W. & Lau, A. Z. Magnetic Resonance Imaging. in *Encyclopedia of Biomedical Engineering* 574–587 (Elsevier, 2019). doi:10.1016/B978-0-12-801238-3.99945-8.
84. Filler, A. The History, Development and Impact of Computed Imaging in Neurological Diagnosis and Neurosurgery: CT, MRI, and DTI. *Nat. Preced.* 1–1 (2009) doi:10.1038/npre.2009.3267.4.
85. Chou, E. T. & Carrino, J. A. chapter 10 - Magnetic Resonance Imaging. in *Pain Management* (eds. Waldman, S. D. & Bloch, J. I.) 106–117 (W.B. Saunders, 2007). doi:10.1016/B978-0-7216-0334-6.50014-5.
86. Lugauer, F. & Wetzl, J. Magnetic Resonance Imaging. in *Medical Imaging Systems: An Introductory Guide* (eds. Maier, A., Steidl, S., Christlein, V. & Hornegger, J.) (Springer, 2018).
87. Worthoff, W. A., Yun, S. D. & Shah, N. J. CHAPTER 1 Introduction to Magnetic Resonance Imaging. 1–44 (2018) doi:10.1039/9781788013062-00001.
88. Hansen, M. S. & Kellman, P. Image reconstruction: an overview for clinicians. *J. Magn. Reson. Imaging JMRI* **41**, 573–585 (2015).
89. Ma, J. Dixon techniques for water and fat imaging. *J. Magn. Reson. Imaging* **28**, 543–558 (2008).
90. Samei, E. & Peck, D. J. *Hendee's Physics of Medical Imaging*. (John Wiley & Sons, 2019).
91. Walker, R. C. *et al.* Introduction to PET Imaging with Emphasis on Biomedical Research. *NeuroToxicology* **25**, 533–542 (2004).
92. Jadvar, H. & Colletti, P. M. Competitive Advantage of PET/MRI. *Eur. J. Radiol.* **83**, 84–94 (2014).
93. Ehman, E. C. *et al.* PET/MRI: Where Might It Replace PET/CT? *J. Magn. Reson. Imaging JMRI* **46**, 1247–1262 (2017).
94. Chen, Y. & An, H. Attenuation Correction of PET/MR Imaging. *Magn. Reson. Imaging Clin. N. Am.* **25**, 245–255 (2017).
95. Rausch, I. *et al.* Standard MRI-based attenuation correction for PET/MRI phantoms: a novel concept using MRI-visible polymer. *EJNMMI Phys.* **8**, 18 (2021).
96. Teuho, J. *et al.* Magnetic Resonance-Based Attenuation Correction and Scatter Correction in Neurological Positron Emission Tomography/Magnetic Resonance Imaging—Current Status With Emerging Applications. *Front. Phys.* **7**, (2020).
97. Anazodo, U. C. *et al.* Feasibility of simultaneous whole-brain imaging on an integrated PET-MRI system using an enhanced 2-point Dixon attenuation correction method. *Front. Neurosci.* **8**, (2015).
98. Strand, R. *et al.* A concept for holistic whole body MRI data analysis, Imiomics. *PLoS ONE* **12**, e0169966 (2017).
99. Zou, K. H. *et al.* Statistical Validation of Image Segmentation Quality Based on a Spatial Overlap Index. *Acad. Radiol.* **11**, 178–189 (2004).

100. Iglesias, J. E. & Sabuncu, M. R. Multi-Atlas Segmentation of Biomedical Images: A Survey. *Med. Image Anal.* **24**, 205–219 (2015).
101. Ronneberger, O., Fischer, P. & Brox, T. U-Net: Convolutional Networks for Biomedical Image Segmentation. *ArXiv150504597 Cs* (2015).
102. Siddique, N., Sidike, P., Elkin, C. & Devabhaktuni, V. U-Net and its variants for medical image segmentation: theory and applications. *IEEE Access* **9**, 82031–82057 (2021).
103. Chen, X., Diaz-Pinto, A., Ravikumar, N. & Frangi, A. Deep learning in medical image registration. *Prog. Biomed. Eng.* (2020) doi:10.1088/2516-1091/abd37c.
104. Islam, K. T., Wijewickrema, S. & O'Leary, S. A deep learning based framework for the registration of three dimensional multi-modal medical images of the head. *Sci. Rep.* **11**, 1860 (2021).
105. Breznik, E., Malmberg, F., Kullberg, J., Ahlström, H. & Strand, R. Multiple comparison correction methods for whole-body magnetic resonance imaging. *J. Med. Imaging Bellingham Wash* **7**, 014005 (2020).
106. (ISMRM 2015) Imiomics: Bringing omics to whole body imaging: Examples in cross sectional interaction between whole-body MRI and non-imaging data. https://archive.ismrm.org/2015/3757.html.
107. Lind, L. Population-based cardiovascular cohort studies in Uppsala. *Ups. J. Med. Sci.* **124**, 16–20 (2019).
108. Boersma, G. J. *et al.* Altered Glucose Uptake in Muscle, Visceral Adipose Tissue, and Brain Predict Whole-Body Insulin Resistance and may Contribute to the Development of Type 2 Diabetes: A Combined PET/MR Study. *Horm. Metab. Res.* **50**, 627–639 (2018).
109. Lind, L., Strand, R., Michaelsson, K., Kullberg, J. & Ahlström, H. Relationship between endothelium-dependent vasodilation and fat distribution using the new 'imiomics' image analysis technique. *Nutr. Metab. Cardiovasc. Dis. NMCD* **29**, 1077–1086 (2019).
110. Strand, R., Kullberg, J., Ahlström, H. & Lind, L. Relationships between plasma levels and six proinflammatory interleukins and body composition using a new magnetic resonance imaging voxel-based technique. *Cytokine* **3**, 100050 (2020).
111. Lind, L., Strand, R., Michaëlsson, K., Ahlström, H. & Kullberg, J. Voxel-wise Study of Cohort Associations in Whole-Body MRI: Application in Metabolic Syndrome and Its Components. *Radiology* **294**, 559–567 (2020).
112. Eriksson, J. W. *et al.* Tissue-specific glucose partitioning and fat content in prediabetes and type 2 diabetes: whole-body PET/MRI during hyperinsulinemia. *Eur. J. Endocrinol.* **184**, 879–889 (2021).
113. Diamanti, K. *et al.* Integration of whole-body [18F]FDG PET/MRI with non-targeted metabolomics can provide new insights on tissue-specific insulin resistance in type 2 diabetes. *Sci. Rep.* **10**, 8343 (2020).
114. Lind, L., Kullberg, J., Ahlström, H. & Strand, R. Relationships between carotid artery intima-media thickness and echogenicity and body composition using a new magnetic resonance imaging voxel-based technique. *PloS One* **16**, e0254732 (2021).
115. Sjöholm, T. *et al.* A whole-body FDG PET/MR atlas for multiparametric voxel-based analysis. *Sci. Rep.* **9**, 6158 (2019).
116. Ekström, S. *et al.* Faster dense deformable image registration by utilizing both CPU and GPU. *J. Med. Imaging Bellingham Wash* **8**, 014002 (2021).

117. Ekström, S., Malmberg, F., Ahlström, H., Kullberg, J. & Strand, R. Fast graph-cut based optimization for practical dense deformable registration of volume images. *Comput. Med. Imaging Graph. Off. J. Comput. Med. Imaging Soc.* **84**, 101745 (2020).
118. Guglielmo, P. *et al.* Validation of automated whole-body analysis of metabolic and morphological parameters from an integrated FDG-PET/MRI acquisition. *Sci. Rep.* **10**, 5331 (2020).
119. Pilia, M. *et al.* Average volume reference space for large scale registration of whole-body magnetic resonance images. *PloS One* **14**, e0222700 (2019).
120. Locke, A. E. *et al.* Genetic studies of body mass index yield new insights for obesity biology. *Nature* **518**, 197–206 (2015).
121. Yengo, L. *et al.* Meta-analysis of genome-wide association studies for height and body mass index in ∼700000 individuals of European ancestry. *Hum. Mol. Genet.* **27**, 3641–3649 (2018).
122. Shungin, D. *et al.* New genetic loci link adipose and insulin biology to body fat distribution. *Nature* **518**, 187–196 (2015).
123. Wen, W. *et al.* Genome-wide association studies in East Asians identify new loci for waist-hip ratio and waist circumference. *Sci. Rep.* **6**, 17958 (2016).
124. Karasik, D. *et al.* Disentangling the genetics of lean mass. *Am. J. Clin. Nutr.* **109**, 276–287 (2019).
125. Wood, A. R. *et al.* Defining the role of common variation in the genomic and biological architecture of adult human height. *Nat. Genet.* **46**, 1173–1186 (2014).
126. Rask-Andersen, M., Karlsson, T., Ek, W. E. & Johansson, Å. Genome-wide association study of body fat distribution identifies adiposity loci and sex-specific genetic effects. *Nat. Commun.* **10**, 339 (2019).
127. Ji, Y. *et al.* Genome-Wide and Abdominal MRI Data Provide Evidence That a Genetically Determined Favorable Adiposity Phenotype Is Characterized by Lower Ectopic Liver Fat and Lower Risk of Type 2 Diabetes, Heart Disease, and Hypertension. *Diabetes* **68**, 207–219 (2018).
128. Liu, Y. *et al.* Genetic architecture of 11 organ traits derived from abdominal MRI using deep learning. *eLife* **10**, e65554 (2021).
129. Sudlow, C. *et al.* UK Biobank: An Open Access Resource for Identifying the Causes of a Wide Range of Complex Diseases of Middle and Old Age. *PLoS Med.* **12**, e1001779 (2015).
130. Naganawa, M. *et al.* Assessment of population-based input functions for Patlak imaging of whole body dynamic 18F-FDG PET. *EJNMMI Phys.* **7**, 67 (2020).
131. Cohen, J. *Statistical Power Analysis for the Behavioral Sciences*. (Routledge, 2013).
132. Hogben, L. T. & Ponder, E. BIOLOGICAL MONOGRAPHS AND MANUALS. 336.

Acta Universitatis Upsaliensis

Digital Comprehensive Summaries of Uppsala Dissertations from the Faculty of Medicine 1846

Editor: The Dean of the Faculty of Medicine

A doctoral dissertation from the Faculty of Medicine, Uppsala University, is usually a summary of a number of papers. A few copies of the complete dissertation are kept at major Swedish research libraries, while the summary alone is distributed internationally through the series Digital Comprehensive Summaries of Uppsala Dissertations from the Faculty of Medicine. (Prior to January, 2005, the series was published under the title "Comprehensive Summaries of Uppsala Dissertations from the Faculty of Medicine".)

Distribution: publications.uu.se
urn:nbn:se:uu:diva-473349

ACTA
UNIVERSITATIS
UPSALIENSIS
UPPSALA
2022